Theoretical Notes

Note 366

2 February 1996

Propagation of Impulse-Like Waveforms Through the Ionosphere Modelled by a Cold Plasma

D. V. Giri

Pro-Tech, 3708 Mt. Diablo Blvd, #215, Lafayette, CA 94549

and

S. L. Dvorak

Department of Electrical & Computer Engineering

The University of Arizona, Tucson, AZ 85721

Abstract

In this note, we have studied the propagation of short, impulse-like pulses propagating through the ionosphere. The ionosphere is modelled by a simple, cold plasma. The impulse response of such a plasma model is known to consist of two terms. The first term is the impulse itself and the second term contains a Bessel function of first order. This means that the impulse propagates as an impulse followed by a long, oscillatory tail. The numerical example studied here is that of the prototype impulse radiating antenna (IRA). Closed-form expressions are developed for the prototype IRA waveform propagation through the cold-plasma model of the ionosphere. The results are cross checked with numerical evaluation via a convolution process that uses the known impulse response.

Preface

The authors wish to thank Dr. Carl E. Baum of Phillips Laboratory for useful discussions. We are also grateful to Dr. D. McLemore of Kaman Sciences Corporation, Dikewood Division, and Mr. Bill Prather, Dr. John Gaudet and Mr. Tyron Tran of Phillips Laboratory for their guidance and support.

Contents

1. Introduction

The emerging ultrawideband or short-pulse technologies will continue to find applications in several forms of radar, target identification, wideband jammers, UXO and perhaps even orbital debris detection. The pulse durations are of the order of 100 ps and the bandwidths range from 10's of MHz to several GHz. All of the current and future UWB applications will involve the interaction of short-pulse electromagnetic waves with earth, water, metallic structures, dielectric surfaces and earth's atmosphere. These objects could be the subjects of radar interogation or may be in the path of radar's interogation. In this note, we are focussing on the interaction of approximate impulses with the ionosphere. Impulse propagation through the earth's atmosphere differs widely from the narrowband propagation. Each frequency component of the approximate impulse is imparted certain magnitude and phase change. The superposition of such effects over broad frequency ranges and large distances can significantly alter the incident electromagnetic pulse. The subject of narrowband propagation through the earth's atmosphere has been intensely investigated ever since Marconi achieved transatlantic communication in 1901. The study of approximate-impulse propagation through the earth's atmosphere is of recent interest e.g., [1 to 4]. When the ionosphere is modelled as a cold plasma with a certain, fixed plasma cut off frequency ω_p, then the dispersion exhibited is similar to that in a single-moded and homogeneously-filled waveguide. The impulse response for this problem can be written in closed form in terms of the impulse function which propagates and is followed by a Bessel function term [2 to 4 among others]. Dvorak and Dudley [2] have also extended the analysis to a double exponential pulse propagating through a cold plasma.

Given the above background, the present goal is to study the propagation of an impulse-like waveform (not exactly an impulse) generated by a reflector IRA in general [5 and 6] and the prototype IRA in particular [7]. To a first-order approximation, we may consider the prepulse and impulse terms of the radiated field in time and frequency domains [8] while ignoring the postpulse term resulting from diffracted signals from the reflector rim and launcher plates.

2. Ionosphere as a Cold Plasma

The ionospheric effects on the information carried by radio waves is legendary and a recent review may be found in [9]. Advances in radar, communication, remote sensing and ionospheric sounding technologies have invoked a lot of propagation studies. The introduction of a sophisticated UWB technology requires an even more detailed investigation of the propagation effects. The ionosphere is a complex, electromagnetically speaking, medium with diurnal, seasonal and long-term variations driven primarily by both solar activity and local disturbances and plasma instabilities. There is a lot of information available and we have summarized in figures 1 and 2, what is relevant for the present study.

To a first order, the earth's atmosphere is horizontally stratified. One of the ways to distinguish the horizontal layers is through the temperature (figure 1). Various physical phenomena such as radiative transport in the infrared, convection cooling near the earth's surface, ultraviolet (UV) absorption by ozone layers in the troposphere etc., determine this temperature profile. It may also be noted that the ionosphere is the charged component of the earth's atmosphere ranging from about 60 km to 1000 km. There is no significant ionization below 60 km. The electron density and the electron collission frequency as a function of the altitude is shown in figure 2. The ion and neutral components of the atmospheric plasma are assumed to be stationary and the maximum value of the electron collission frequency is seen to be about 100 kHz at an altitude of 60 km. For impulse-like waveforms, whose frequency content starts in HF and goes up into S-band, the propagation through the ionosphere is essentially collissionless, consequently lossless. Messier [1] has developed an expression for these losses due to electronic collissions, given by

$$A(dB/m) \simeq 7.28 \times 10^{-6} \left[\frac{N\nu}{f^2 + \nu^2} \right] \tag{1}$$

where

N = electron density (m^{-3})

ν = electron collission frequency (Hz)

f = frequency of the propagating wave (Hz)

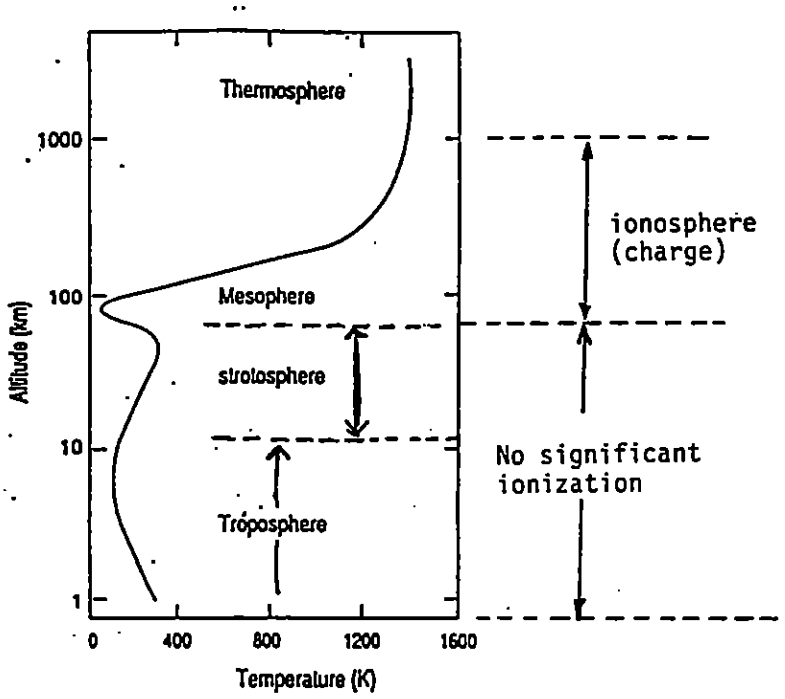

Figure 1. Atmospheric temperature as a function of altitude [9]

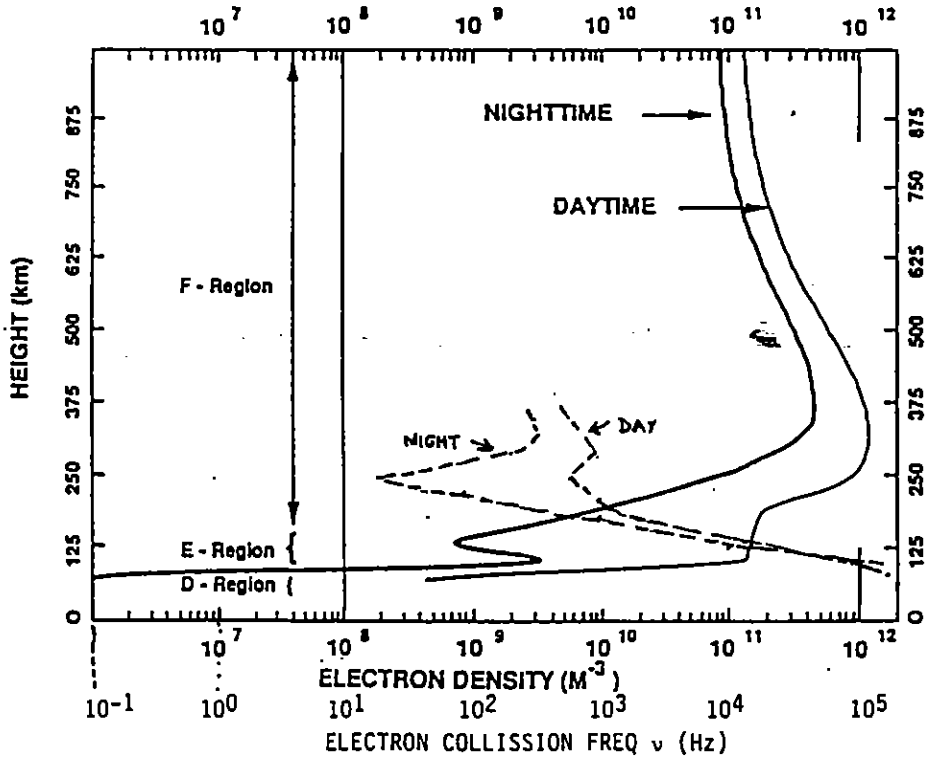

Figure 2. The electron density N and collission frequency ν (Hz) profiles of the ionosphere [9]

Since $f \gg \nu$, using the highest $\nu = 100$ KHz, the attenuations are 3.64×10^{-4} dB/m at $f = 100$ MHz and 3.64×10^{-6} dB/m at $f = 1$ GHz. Over large propagation paths, the effects of electronic collissions leading to ohmic losses have some effect for frequencies below 100 MHz. In this note, we have ignored the effects of collissions since the short-pulse transmission under consideration has spectral magnitudes predominantly in the 100 MHz to 2 GHz band.

Furthermore, when the short-pulse waveform hits the D-layer of the ionosphere at an altitude of about 60 km, part of the incident wave is reflected at this air-ionosphere (charged medium) interface. It is well known that the ionosphere acts like a high-pass filter where the frequencies below the plasma frequency ω_p are reflected and frequencies above ω_p are transmitted. In other words, one could model the ionosphere as a cold-plasma with a plasma frequency of ω_p given by

$$\omega_p = \sqrt{\frac{Ne^2}{m\varepsilon_0}} \simeq 56.37\sqrt{N} \qquad (2)$$

$$\text{or } f_p = \frac{\omega_p}{2\pi} \simeq 8.97\sqrt{N} \text{ Hz}$$

where

$N \equiv$ electron density in (m^{-3})

$e \equiv$ electronic charge $\simeq 1.602 \times 10^{-19}$ C

$m \equiv$ electronic mass $\simeq 9.108 \times 10^{-31}$ kg

$\varepsilon_0 \equiv$ permittivity of free space $\simeq [1/(36\pi)]$ nF/m

Since the maximum value of N is 10^{12} electrons/m^3, the maximum value of plasma frequency f_p is seen to be about 9 MHz. Once again, the significant frequencies of interest in the propagation of impulse-like waveforms are significantly above the plasma frequency f_p and certainly above the collission frequency ν.

In addition to the effects discussed above, the propagation of the short-pulse waveforms is also affected by the earth's magnetic field and refractive bending at non-normal incidence.

The effect of the earth's magnetic field is to render the ionosphere plasma medium into a birefringent, non-reciprocal medium resulting in two values of refractive index. The net effect is to decompose the incident linearly polarized electromagnetic wave into left and right circularly polarized components, also termed as the 'ordinary' and 'extraordinary' waves [10]. For the present, we have neglected the geomagnetic field effects. The refractive bending is predominant at frequencies near ω_p. It has been ignored here since ($\omega \gg \omega_p$) and can be included in future studies. Simply stated the approximations made here are:

a) the ionosphere is modelled by a cold-plasma or a slab model with a plasma frequency of ω_p, independent of time and bounded by two values for changes with altitude, (a slab model)

b) reflection coefficient at the air-ionosphere surface is 1 below ω_p and 0 above ω_p,

c) geomagnetic field and refractive bending effects are ignored.

Under these assumptions, the geometry of the problem now becomes simple and is shown in figure 3. θ is seen to be the polar angle of launch of the impulse-like waveform transmitter. z_0 is the vertical height of the uncharged, air medium which is roughly 60 km. The propagation distance is $z_0 \sec(\theta)$ in air and $z \sec(\theta)$ in the ionosphere. $z = 0$ plane is the air-ionosphere interface. When the electromagnetic wave radiated from the transmitter on ground is incident at this interface, only the frequencies $> \omega_p$ are transmitted into the charged medium. With reference to the electron-density profile shown in figure 2, we consider two boundary values of $N_1 = 1.12 \times 10^6/m^3$ and $N_2 = 1.12 \times 10^{12}/m^3$ which correspond to low and high values of $\omega_p \simeq 6 \times 10^4$ and 6×10^7. In effect, we have modelled the ionosphere by two values of $f_p \simeq 9.54$ kHz and 9.54 MHz. This is similar to the dispersive wave propagation in a waveguide and the plasma frequency is analogous to the cutoff frequency of the dominant mode of propagation. Both the waveguide and the ionosphere behave like a high-pass filter.

With the ionospheric model described above, we are now in a position to briefly review its impulse response in the following section.

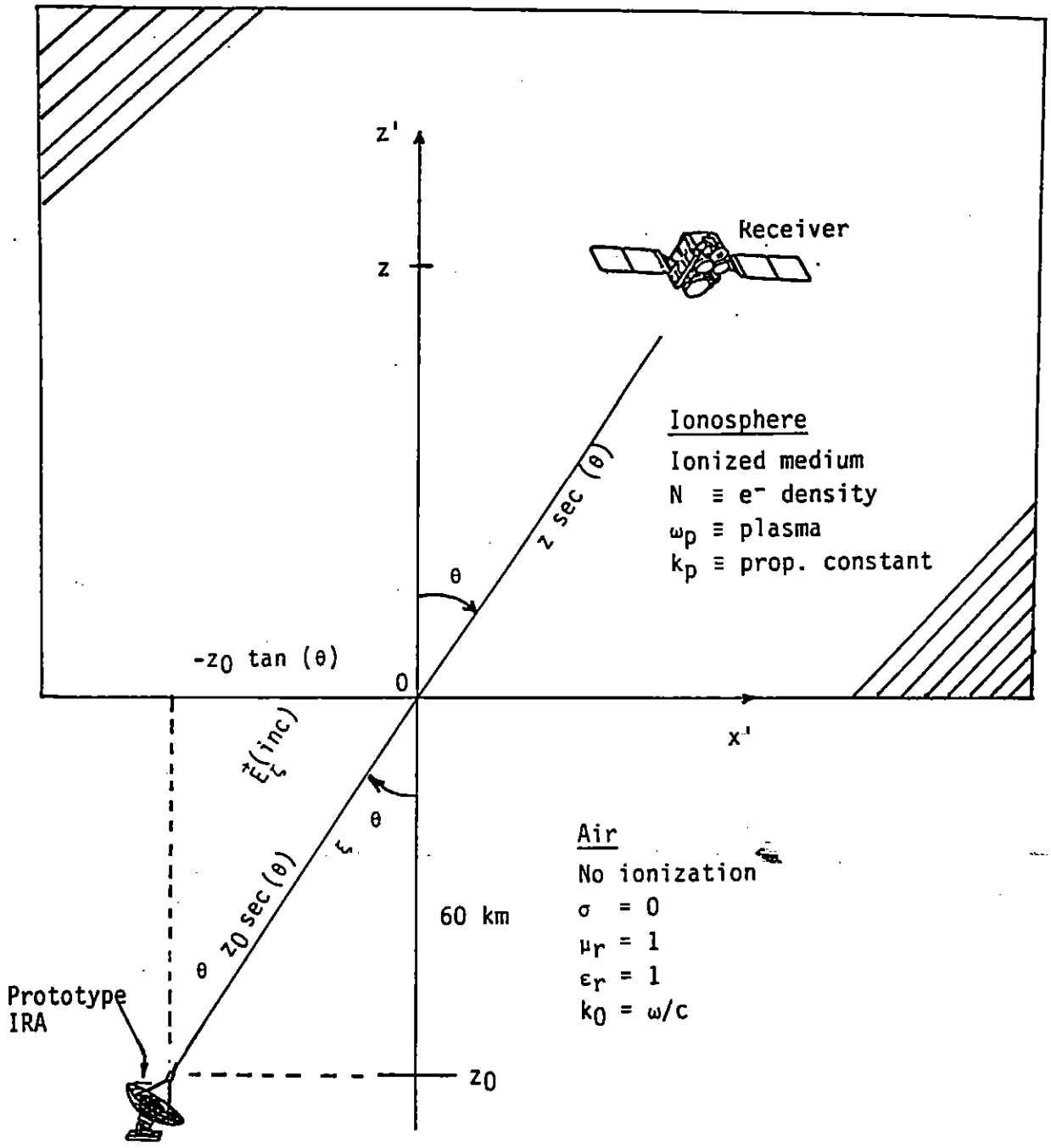

Figure 3. Geometry of the problem

3. Brief Review of the Impulse Response of a Cold Plasma Medium

Under the assumption of a homogeneous, cold-plasma model, the ζ-polarized electric field, propagating in the direction of ξ must satisfy the harmonic equation

$$\left(\frac{d^2}{d\xi^2} + k_\xi^2\right) \quad \tilde{E}_\zeta(\xi, \omega) = 0 \tag{3}$$

where $k_\xi = \sqrt{k_0^2 - k_p^2}$, $k_0 = \omega\sqrt{\mu_0\varepsilon_0}$ and $k_p = \omega_p\sqrt{\mu_0\varepsilon_0}$.

The plasma cutoff frequency ω_p is related to the electron density as indicated in (2). The general solution for the above differential equation is

$$\tilde{E}_\zeta(\xi, \omega) = \tilde{E}_\zeta(0, \omega) \ \left[e^{-jk_\xi\xi} + \Gamma\, e^{jk_\xi\xi}\right] \tag{4}$$

Numerous researchers have shown that the impulse response of a waveguide or a cold plasma can be expressed in closed form in terms of the Bessel function of the first kind, [e.g., 2 to 4]. Under the assumption of no reflection ($\Gamma = 0$) valid for $\omega > \omega_p$, (4) reduces to

$$\tilde{E}_\zeta(\xi, \omega) = \tilde{E}_\zeta(0, \omega)\ e^{-j(\xi/c)\sqrt{\omega^2-\omega_p^2}} \tag{5}$$

or, in time domain

$$E_\zeta(\xi, t) = \frac{1}{2\pi}\int_{-\infty}^{\infty} \tilde{E}_\zeta(0, \omega)\, e^{j\left[\omega t - \frac{\xi}{c}\sqrt{\omega^2-\omega_p^2}\right]}\, d\omega \quad ;\xi > 0 \tag{6}$$

For an impulse function input $E_\zeta(0, t) = \tilde{E}_0\, \delta(t)$, we have $\tilde{E}_\zeta(0, \omega) = \tilde{E}_0\ (V - s/m)$, the above equation becomes

$$E_\zeta(\xi, t) = \frac{\tilde{E}_0}{2\pi}\int_{-\infty}^{\infty} \exp\left\{j\left[\omega t - \frac{\xi}{c}\sqrt{\omega^2 - \omega_p^2}\right]\right\} d\omega \tag{7}$$

Using the Fourier integral representation of a Bessel function [11],

$$J_0(\omega_p\sqrt{t^2-(\xi/c)^2})\;u\left(t-\frac{\xi}{c}\right)=\frac{1}{2\pi j}\int_{-\infty}^{\infty}\frac{e^{j\left[\omega t-\left(\frac{\xi}{c}\right)\sqrt{\omega^2-\omega_p^2}\right]}}{\sqrt{\omega^2-\omega_p^2}}\,d\omega \tag{8}$$

we have, for the impulse response

$$\begin{aligned}E_\zeta(\xi,t)&=-\tilde{E}_0\frac{\partial}{\partial(\xi/c)}\;J_0(\omega_p\sqrt{t^2-(\xi/c)^2})\;u(t-\xi/c)\\&=\tilde{E}_0\left[\delta\left(t-\frac{\xi}{c}\right)-u\left(t-\frac{\xi}{c}\right)\;\frac{\omega_p\xi J_1(\omega_p\sqrt{t^2-(\xi/c)^2}}{c\sqrt{t^2-(\xi/c)^2}}\right]V/m\\&=\tilde{E}_0\left[\delta\left(t-\frac{\xi}{c}\right)-u\left(t-\frac{\xi}{c}\right)\;\frac{k_p\xi J_1(\omega_p\sqrt{t^2-(\xi/c)^2}}{\sqrt{t^2-(\xi/c)^2}}\right]V/m\end{aligned} \tag{9}$$

This result is well established and is available in the literature [2 to 4]. However, some comments about the impulse response are in order. We observe that after propagating through a distance ξ in the cold plasma, the incident impulse $\tilde{E}_0\delta(t)$ reappears, but is followed by an oscillatory behavior in time, which is represented by the first-order Bessel function term. Herein lies the clue for the propagation of the impulse-like waveform radiated by a reflector IRA. The radiated waveform from the IRA is an approximate impulse $\delta_a(t)$ and not an exact impulse. The reason that the exact impulse propagates through the cold plasma, unperturbed is because it has infinite energy. One may expect for an approximate impulse propagation, that the initial peak would propagate but compressed in duration due to the interaction term with the Bessel function portion. It would then be followed by an oscillatory behavior. In summary, we would expect a time-domain waveform that is highly peaked, followed by a negative undershoot which in turn is followed by an oscillatory behavior. At late times, the period of this oscillation should approach the plasma-oscillation period.

In the next section, we look at the incident fields radiated from a reflector IRA (e.g., the prototype IRA [7 and 8]) and striking the air-ionosphere interface. That is, these are

fields radiated from the prototype IRA that have propagated a distance of $z_0 \sec(\theta)$ where $z_0 = 60$ km and θ is the polar launch angle.

4. Propagation of IRA Fields Through Cold Plasma

Since the propagation distance in air is $z_0 \sec(\theta)$ (see figure 3), the electric field at the air-ionosphere interface from a reflector IRA may be written as [8],

$$\bar{E}_\zeta(\xi, t) = \frac{V_0}{z_0 \sec(\theta)} \frac{D}{4\pi c f_g} \left[\frac{\partial V(t'-T)}{\partial t} - \frac{1}{T}\{V(t') - V(t'-T)\} \right] \tag{10}$$

Note that this field is at $z = 0$, and

$$\begin{aligned} t' &= t - \frac{z_0 \sec(\theta)}{c} \quad , \quad T = 2F/c \\ V(t) &= V_0(e^{-\beta t} - e^{-\alpha t})\, u(t) \equiv \text{voltage waveform} \\ F &\equiv \text{focal length of the paraboloidal reflector} \\ D &\equiv \text{diameter of the paraboloidal reflector} \\ c &\equiv \text{speed of light} \simeq 3 \times 10^8 \ m/s \\ f_g &\equiv Z_{feed}/Z_0 \equiv \text{geometrical factor} \\ Z_{feed} &\equiv \text{TEM feed impedance} \\ Z_0 &\equiv \text{characteristic impedance of free space} \end{aligned} \tag{11}$$

Substituting for $V(t)$ from (11) into (10), we find the electric field at the air-ionosphere interface ($z = 0$) in time and frequency domains to be

$$E_\zeta(z=0, t) = \frac{V_0}{z_0 \sec(\theta)} \frac{D}{4\pi c f_g} \left[\left\{ \alpha\, e^{-\alpha(t'-T)} - \beta\, e^{-\beta(t'-T)} \right\} u(t'-T) \right.$$

$$\left. - \frac{1}{T} \left\{ \left(e^{-\beta t'} - e^{-\alpha t'} \right) u(t') - \left[e^{-\beta(t'-T)} - e^{-\alpha(t'-T)} \right] u(t'-T) \right\} \right] \tag{12}$$

$$\tilde{E}_\zeta(0, \omega) = \frac{\tilde{V}(\omega)}{z_0 \sec(\theta)} \frac{D}{4\pi c f_g} e^{-j\omega t_0} \left[j\omega e^{-j\omega T} - \frac{1}{T}\left\{1 - e^{-j\omega T}\right\} \right] \tag{13}$$

with

$$t_0 = z_0 \sec(\theta)/c \quad \text{and} \quad \tilde{V}(\omega) = V_0 \left[\frac{1}{j\omega + \beta} - \frac{1}{j\omega - \alpha} \right] \tag{14}$$

Equations (12) and (13) completely specify the electric field incident at the air-ionosphere interface in time and frequency domain. These two equations are used in the following sections for the purpose of numerical evaluation relating tothe prototype IRA.

For the present, we continue the formulation of propagating the above described incident field in the ionosphere. The propagation constant in the ionosphere, as before is

$$k_\xi = \frac{1}{c} \sqrt{\omega^2 - \omega_p^2 + j\nu\omega_p^2/\omega} \tag{15}$$

Ignoring the electronic collission frequency ($\nu \ll \omega$) as before,

$$k_\xi = \frac{1}{c} \sqrt{\omega^2 - \omega_p^2} = \frac{\omega}{c} \sqrt{1 - (\omega_p/\omega)^2} = \frac{\omega n}{c} = k_0 n \tag{16}$$

with $n \equiv$ index of refraction and $k_0 \equiv$ propagation constant in free space

Therefore, the spectral domain field after propagating a distance of $z \sec(\theta)$ in the ionosphere is given by

$$\tilde{E}_\zeta(z, \omega) = \frac{\tilde{V}(\omega)}{(z + z_0)\sec\theta} \, e^{-\frac{j\omega}{c}[z_0 \sec(\theta)]} \, e^{-\frac{j\omega}{c}[z_0 \sec(\theta)]\sqrt{1-(\omega_p^2/\omega^2)}}$$

$$\left[j\omega e^{-j\omega T} - \frac{1}{T}\left(1 - e^{-j\omega T}\right) \right] \tag{17}$$

The above frequency-domain field needs to be Fourier inverted to obtain time-domain electric field. However, noting the form of $\tilde{V}(\omega)$ given in (14), we define

$$e(u,\,t) = \frac{1}{2\pi j}\int_{-\infty}^{\infty} \frac{e^{j\omega t}\; e^{-j\frac{z}{c}\sec(\theta)\sqrt{\omega^2-\omega_p^2}}}{(\omega - ju)}\; d\omega \tag{18}$$

then the Fourier inversion of (17) leads to

$$\begin{aligned} E_\zeta(z,\,t) &= \frac{V_0}{(z+z_0)\sec(\theta)}\;\frac{D}{4\pi c f_g\, T}\; F(t) \\ &= \frac{V_0}{(z+z_0)\sec(\theta)}\;\frac{1}{8\pi f_g f_d}\; F(t) \end{aligned} \tag{19}$$

where $f_d = F/D$ and $F(t)$ is given by

$$F(t) = [\{(1-\beta T)e(\beta,\,t-t_0-T) - e(\beta,\,t-t_0)\} - \{(1-\alpha T)e(\alpha,\,t-t_0-T) - e(\alpha,\,t-t_0)\}] \tag{20}$$

recalling $e(u,\,t)$ is given in (18) and

$$\begin{aligned} t_0 &= z_0\,\sec(\theta)/c \\ T &= 2F/c \end{aligned} \tag{21}$$

It is also observed that $e(u,\,t)$ defined in (18) can be expressed in terms of certain special functions termed incomplete Lipschitz-Hankel (IL-H) functions [12] that have integral representation in terms of the well known Bessel functions. This relation of the $e(u,\,t)$ with IL-H functions or integrals is useful in numerical computation of the fields received by a receiver in the ionosphere. Equations (17) in frequency domain and (19) in time-domain formally provide the closed-form expressions for the fields in the ionosphere for a reflector IRA transmitter on the ground.

5. Incident IRA Waveforms and Spectra

While the previous sections have formulated the problem and developed closed-form expressions for the wave propagation through the ionosphere modelled as a cold plasma, we illustrate this propagation with numerical examples in this and the following section. Specifically, we consider the electromagnetic fields radiated from the prototype IRA [7 and 8]. The geometry of this electromagnetic short-pulse launch from earth to its atmosphere is depicted in earlier figure 3. The boresight, electric field radiated by the prototype IRA is expressed in (12) and (13) in time and frequency domains. The equations are suitably modified [8] for the case of four-arm feed. The following numerical values are considered in this illustration.

Antenna Parameters

$D = 3.66$ m $\quad F = 1.2$ m $\quad \Rightarrow\ T = 2F/c \simeq 8$ ns

$Z_{feed} \simeq 400\Omega \quad f_g = 1.06 \quad$ (2 arms)

$f_d = F/D = 0.33$

Pulser Parameters

$V_0 = 10^5$ V $\quad \beta \simeq 5 \times 10^7/s \quad \alpha \simeq 2.2 \times 10^{10}/s$

t_{10-90} (rise) $\simeq 100$ ps $\quad t_{e-fold}$(decay) $\simeq 20$ ns

Propagation in air

$z_0 = 60$ km

$\theta_i = 0,\ 15°,\ 30°,\ 45°,\ 60°$ and $75°$

Propagation in the Ionosphere

$$\left\{ \begin{array}{l} N_i = 1.12 \times 10^6\ (\mathrm{m}^{-3}) \quad \text{and} \quad 1.12 \times 10^{12}\ (\mathrm{m}^{-3}) \\ \omega_p = 6 \times 10^4\ (\mathrm{rad/s}) \quad \text{and} \quad 6 \times 10^7\ (\mathrm{rad/s}) \\ f_p = 9.54\ \mathrm{kHz} \quad \text{and} \quad 9.54\ \mathrm{MHz} \end{array} \right\}$$

$z = 500,\ 600,\ 700$ and 800 km.

As a first step, we present the fields incident at the air-ionosphere interface in time and frequency domains. The antenna and the pulser parameters are fixed and the vertical distance to the D-layer is also fixed at $z_0 = 60$ km. The previously measured time-domain

electric field at a distance of 304 m and the computed spectrum are shown in figure 4. The launch angle measured from the vertical is varied from 0 to 75° in steps of 15° and the resulting incident fields from the prototype IRA (with an rE factor of $\sim$ 1220 kV) are shown in figures 5 to 10. Figures 5 to 10 are simply scaled versions of figure 4 following the $(1/r)$ fall off from the antenna. While the time-domain field in figure 4 is a measured waveform, the fields in figures 5 to 10 are estimated and ignore the small, postpulse components of the waveform. The prepulse is significant and visible at a distance of 304 m and falls of like $(1/r)$. It is also observed that the negative area of the prepulse is cancelled out by the impulse area as evidenced by the spectral graphs where the spectral magnitude approaches zero at dc.

The time-domain and spectral magnitude of the electric field incident at the air-ionosphere interface at a height of 60 km are summarized in figure 11, for varying angles of launch. These fields are then propagated through the ionosphere using the formulation of section 4.

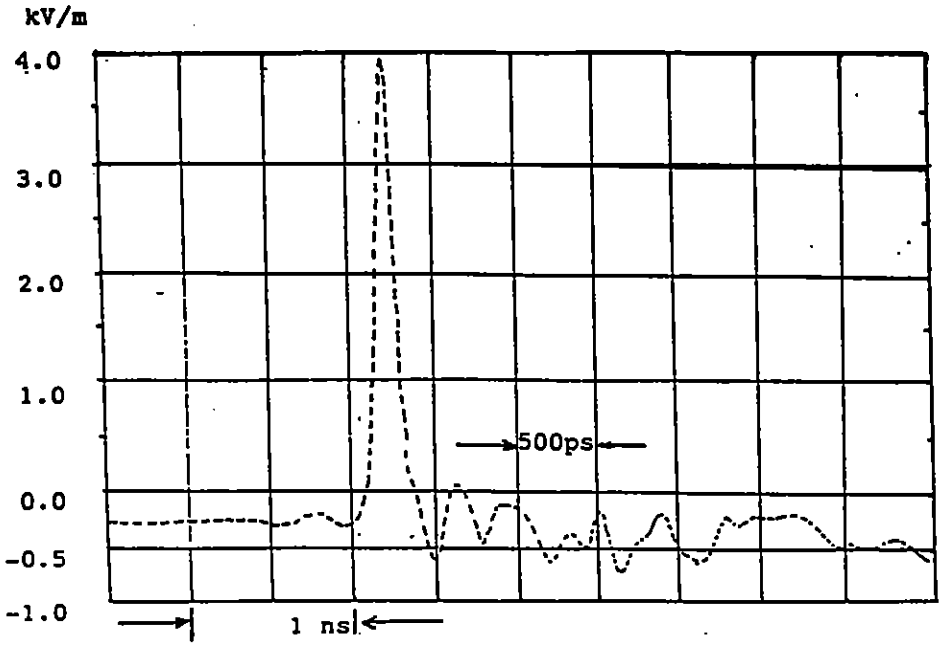

a) time-domain

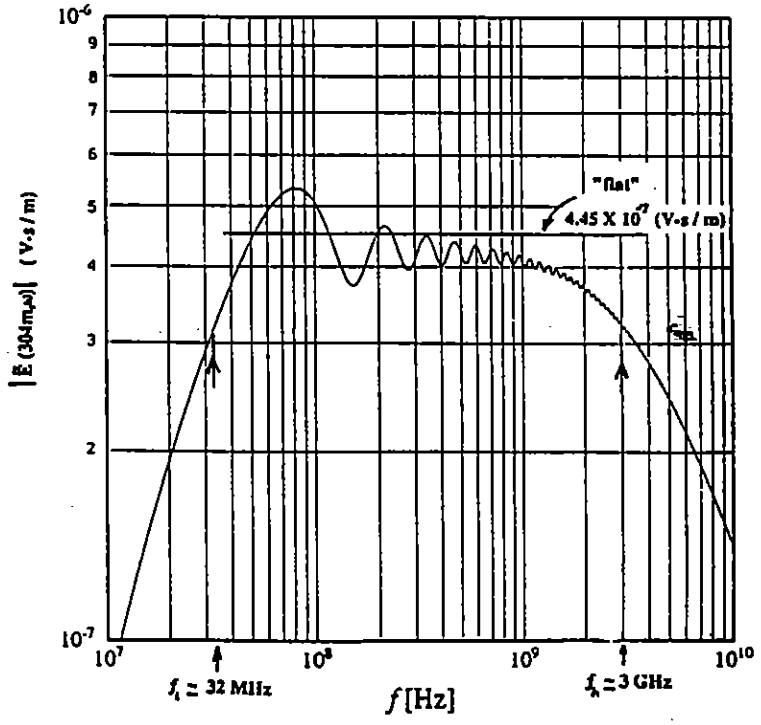

b) frequency-domain

Figure 4. On-axis electric field from the Prototype IRA at a distance of 304 m

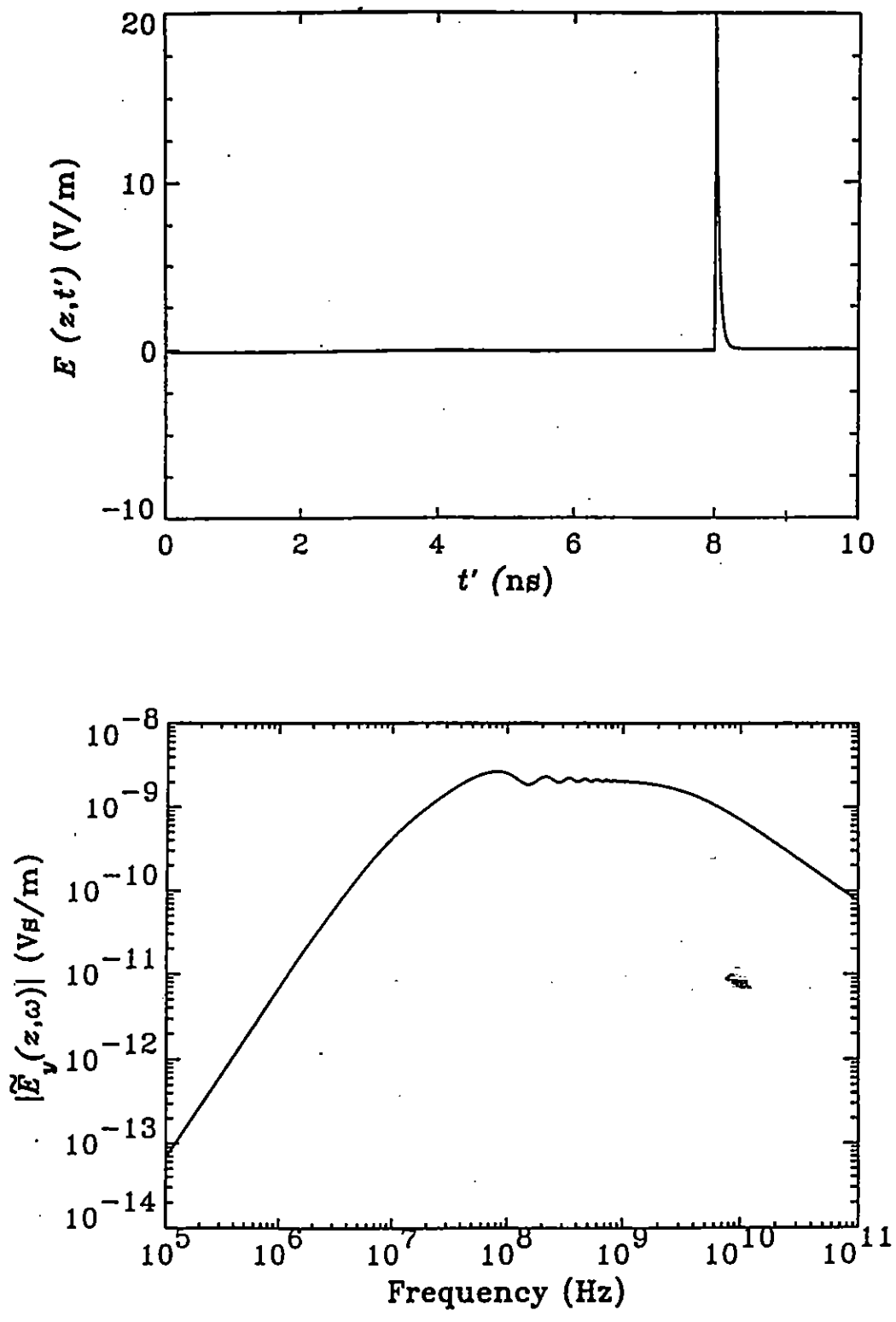

Figure 5. The electric field incident at the air-ionosphere interface ($z_0 = 60$ km; $z = 0$ and $\theta = 0°$)

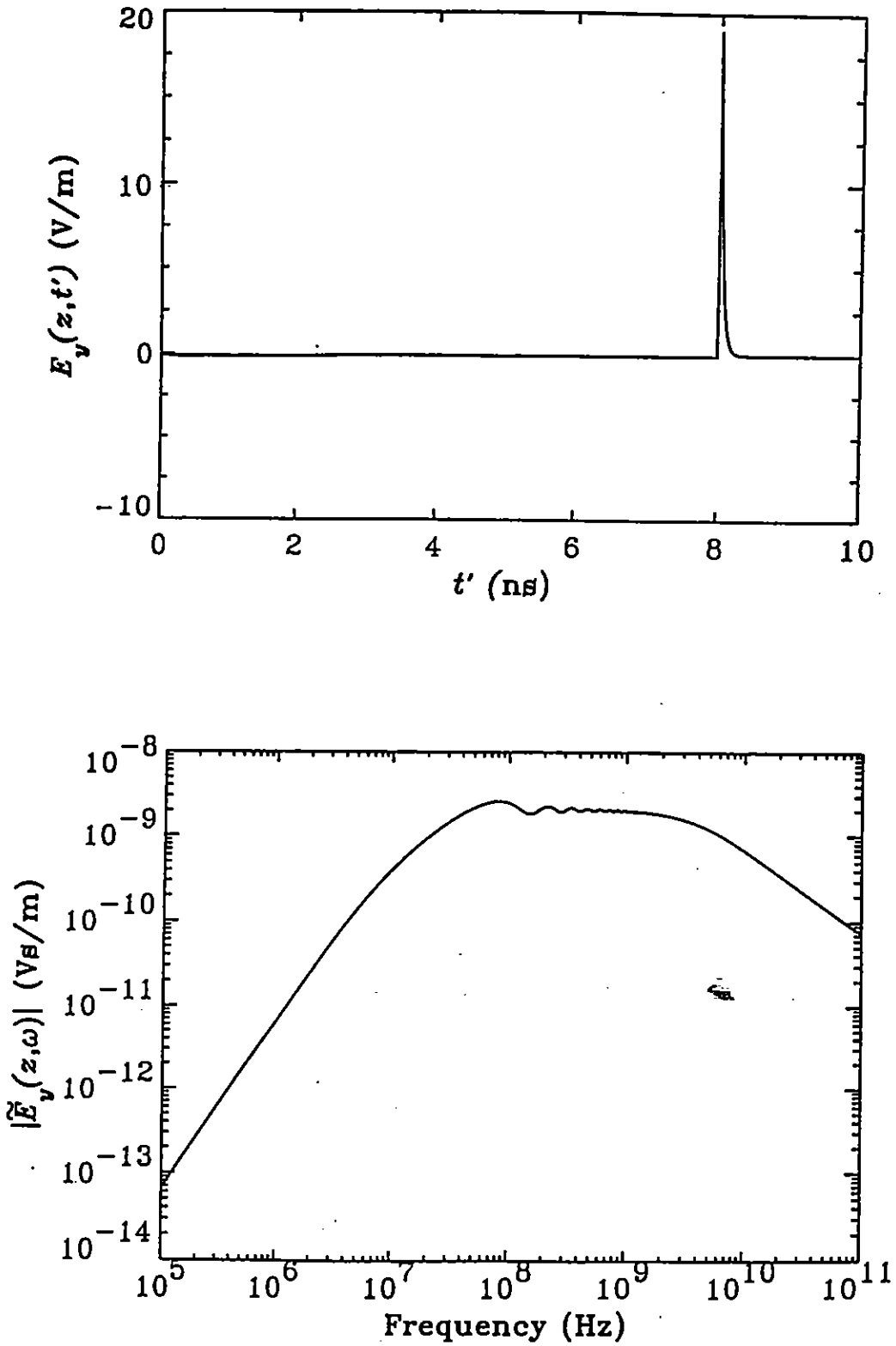

Figure 6. The electric field incident at the air-ionosphere interface ($z_0 = 60$ km; $z = 0$ and $\theta = 15°$)

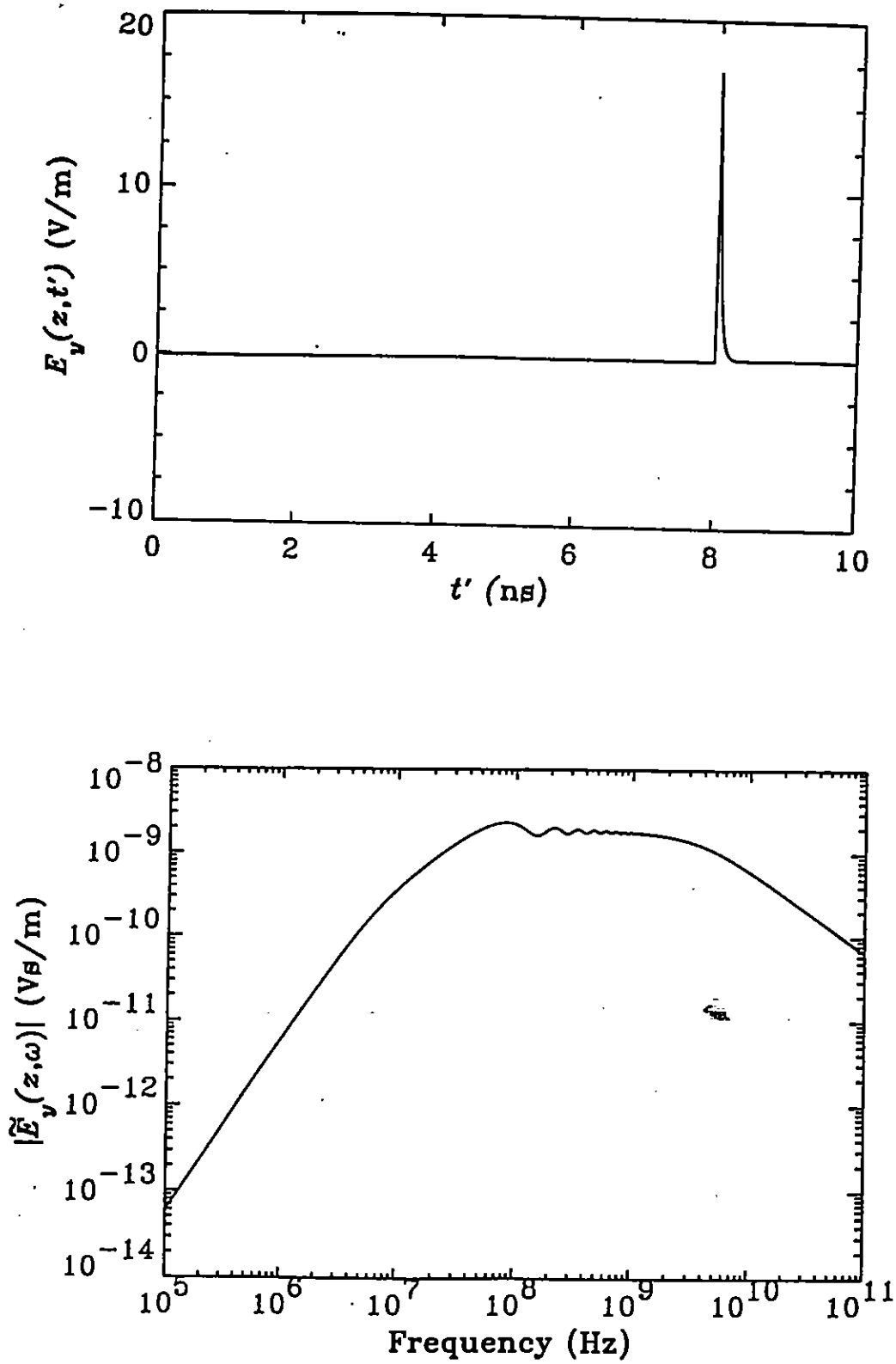

Figure 7. The electric field incident at the air-ionosphere interface ($z_0 = 60$ km; $z = 0$ and $\theta = 30°$)

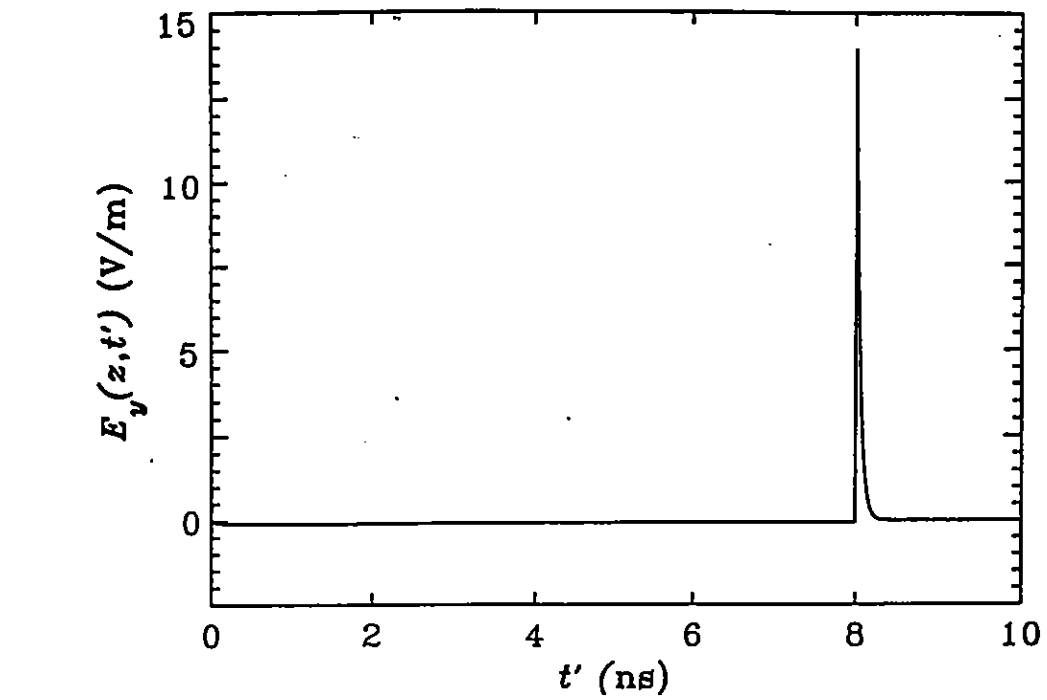

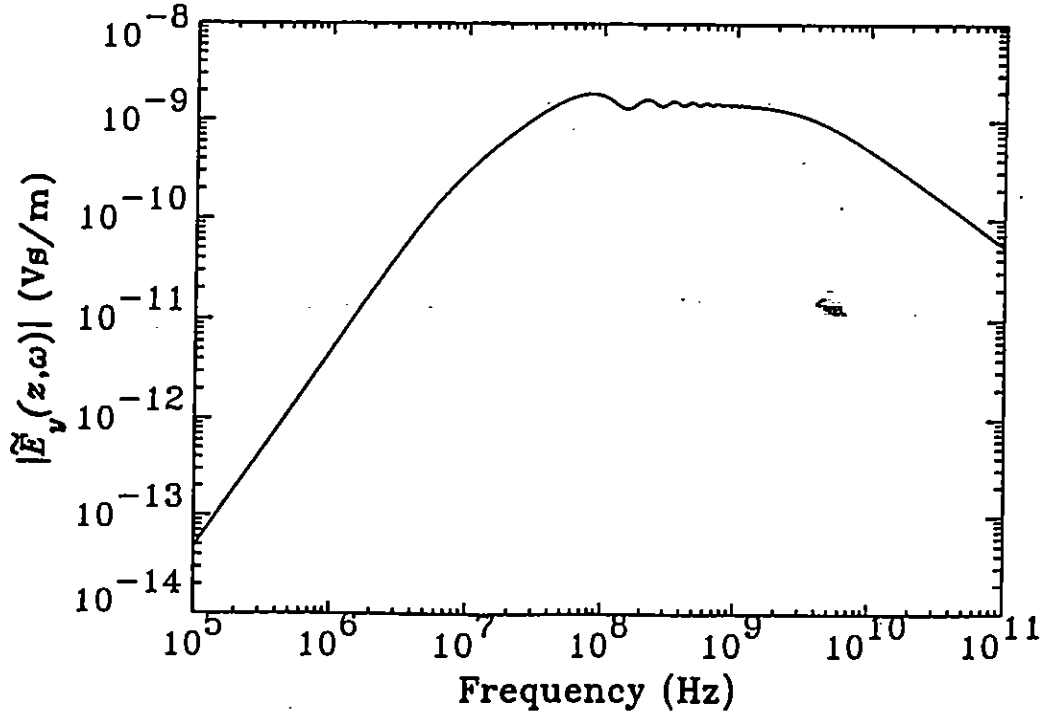

Figure 8. The electric field incident at the air-ionosphere interface ($z_0 = 60$ km; $z = 0$ and $\theta = 45°$)

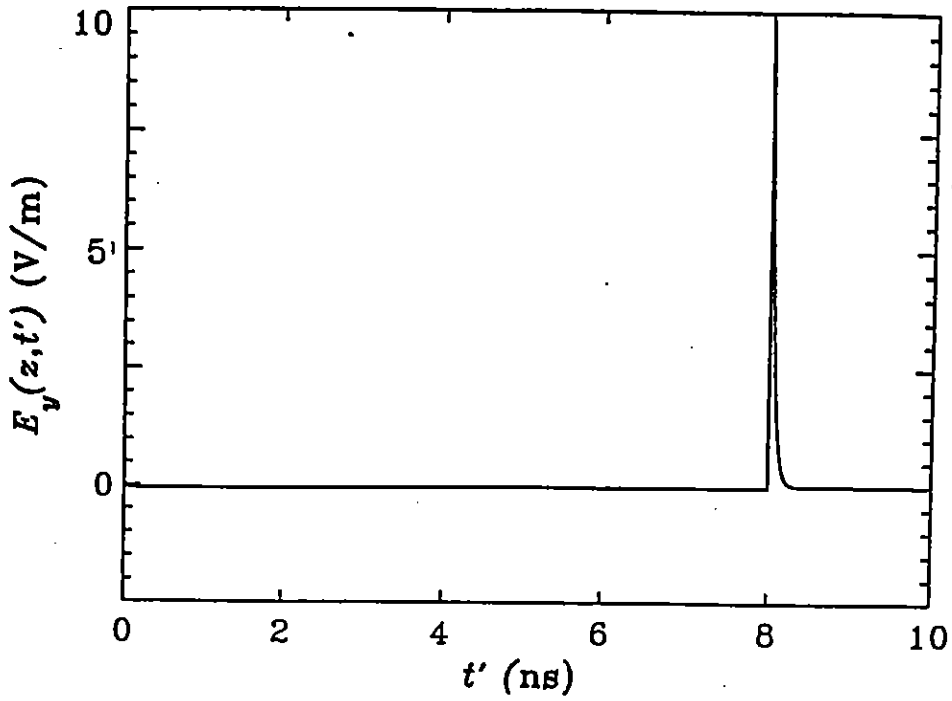

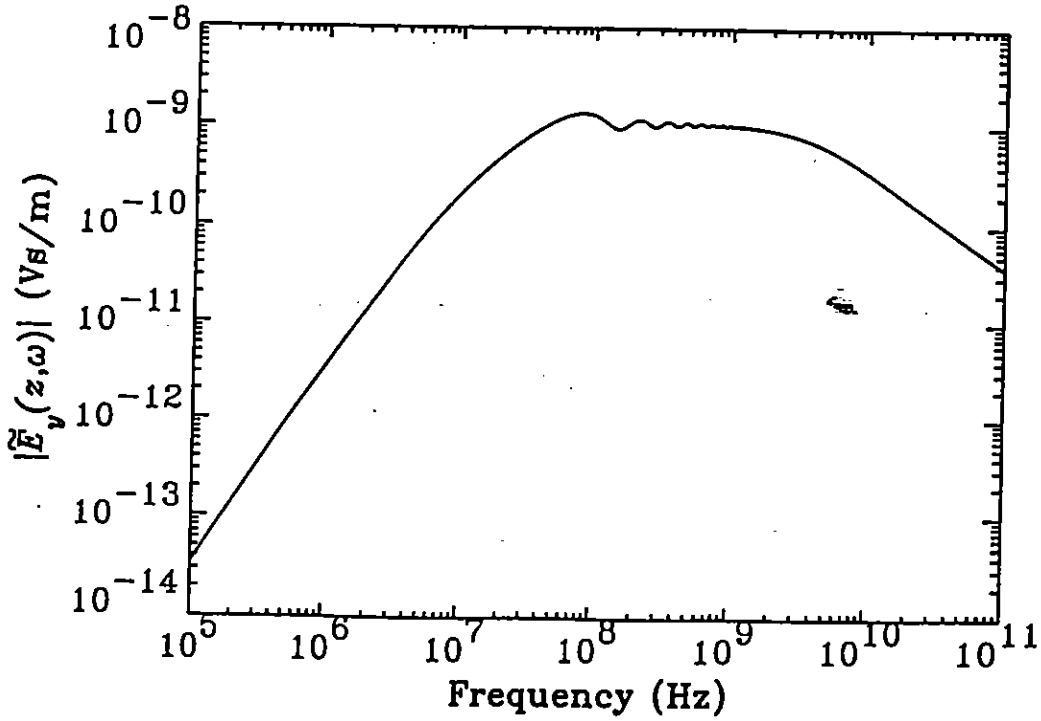

Figure 9. The electric field incident at the air-ionosphere interface ($z_0 = 60$ km; $z = 0$ and $\theta = 60°$)

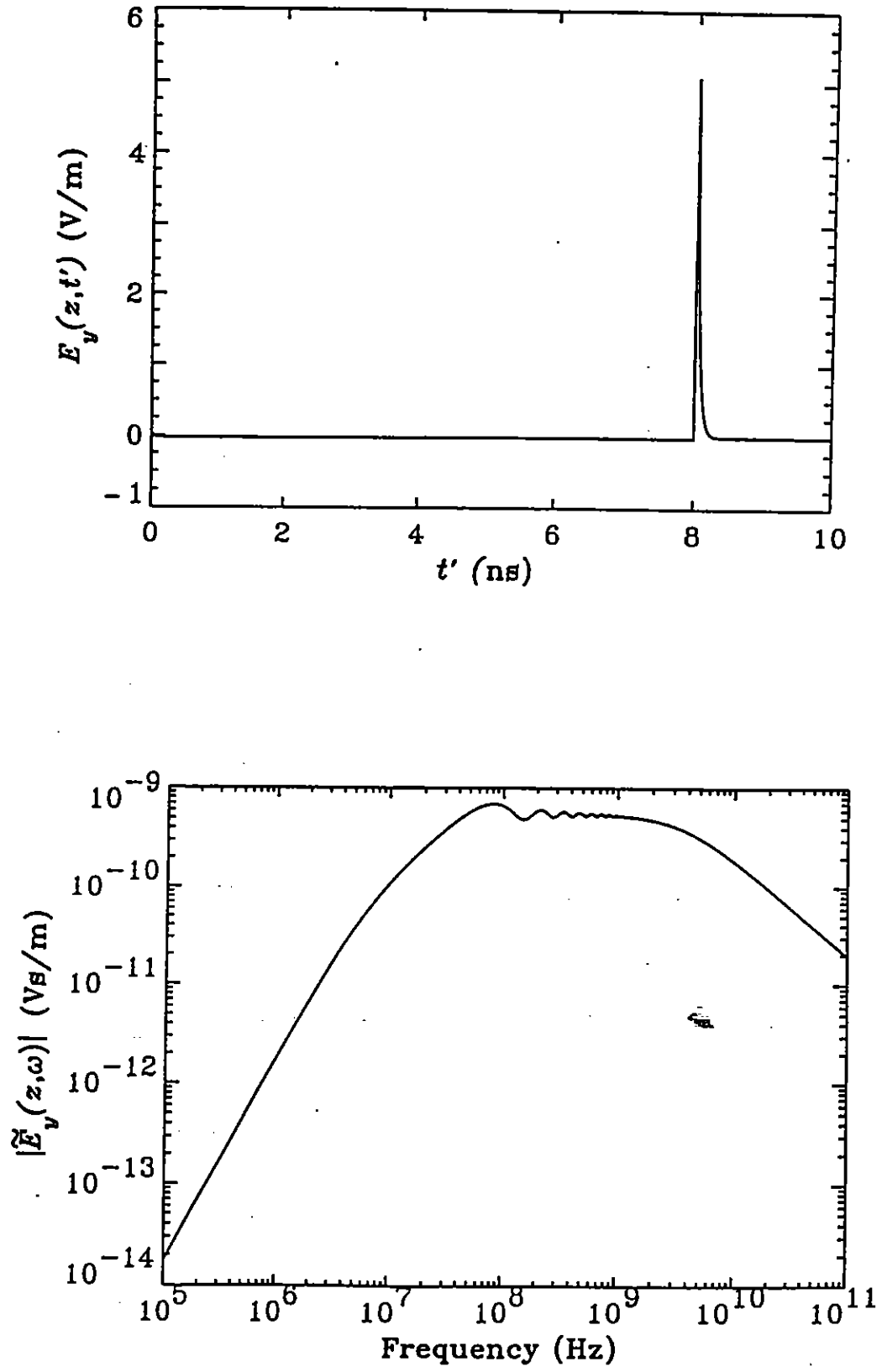

Figure 10. The electric field incident at the air-ionosphere interface ($z_0 = 60$ km; $z = 0$ and $\theta = 75°$)

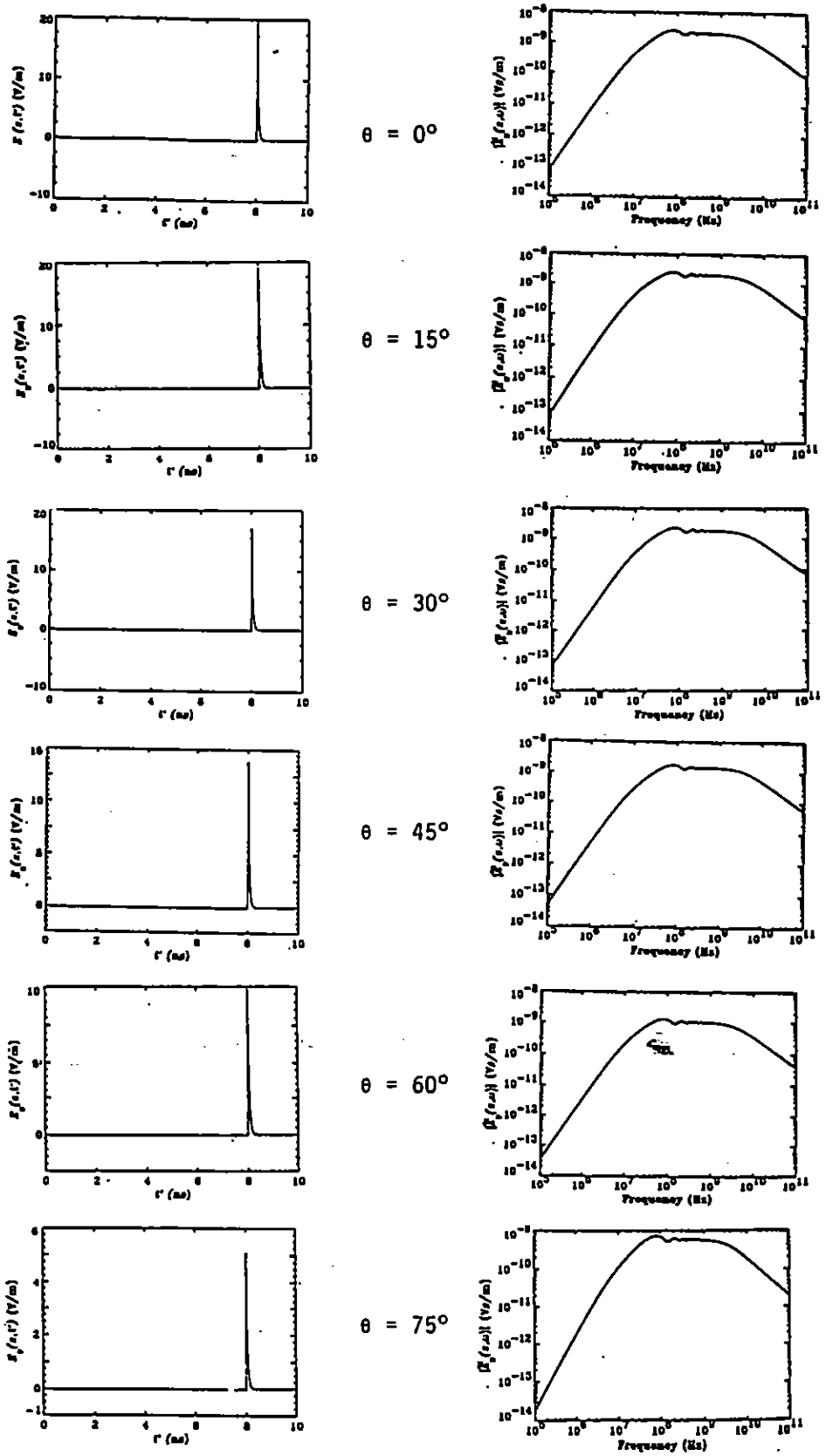

Figure 11. Electric field incident at the air-ionosphere interface for varying launch angles

6. Numerical Results for the Prototype IRA

In this section, we consider four values of the "slab" thicknesses for the ionosphere as mentioned earlier. These are the four vertical distances z_i = 500, 600, 700 and 800 km. Note that these distances are measured from the air-ionosphere interface and one would add 60 km to obtain vertical height above the earth's surface. We have also considered a homogeneous (i.e., electron density not varying with height) cold plasma with 2 values that bound the problem.

A. Plasma frequency $f_p \simeq 9.54\ kHz$

This case corresponds to an electron density N of 1.12×10^6 electrons/m^3 or $\omega_p \simeq 6 \times 10^4$ or $f_p \simeq 9.54$ kHz. We compute both frequency and time-domain signals, after trans-ionospheric propagation. The time domain signals are plotted in figures 12 to 17. The main feature of trans-ionospheric propagation for the chosen value of $N \simeq 1.12 \times 10^6/m^3$ is that the IRA pulse propagates, with minimal distortion. We may look at a specific case of z = 500 km for example, in greater detail. Figure 18 shows a long-time history of the trans-ionospheric propagation and highlights the presence of the prepulse. The peak value of the impulse is out-of scale in this figure. It is observed that the prepulse lasts for about 8 ns ($\simeq 2F/c$) as expected. The spectral magnitude of the electric field for the case of z = 500 km; $f_p \simeq 9.54$ kHz and $\theta = 0$ is shown in figure 19. The plasma cutoff frequency is so low that the spectrum is unaffected. Changing the values of z and θ only multiplies this spectrum by a contant C_1. C_1 is simply given by [cos(θ) $\times$ 500 km/z] with $C_1 = 1$ for $\theta = 0$ and z = 500 km. Figure 19 will then be the frequency domain signal [V/(m – Hz)] incident on a receiver in the ionosphere. The actual signal at the receiver terminals is a function of receiver's sensitivity, bandwidth, etc.

We now turn our attention to the additional (other than $1/r$) losses in the ionosphere due to electron collissions. The results of figures 12 to 19 do not include the effect of ohmic losses due to collissions. Recall that in the frequency-domain, the losses are given by (1) and the spectral magnitudes of the received signals with and without losses for z = 500 km and $\theta = 0°$ are shown in figure 20. The ohmic losses due to electron collissions fall off like $(1/f^2)$ and are negligible above 1 MHz, even for large propagation paths of 500 to 800 km.

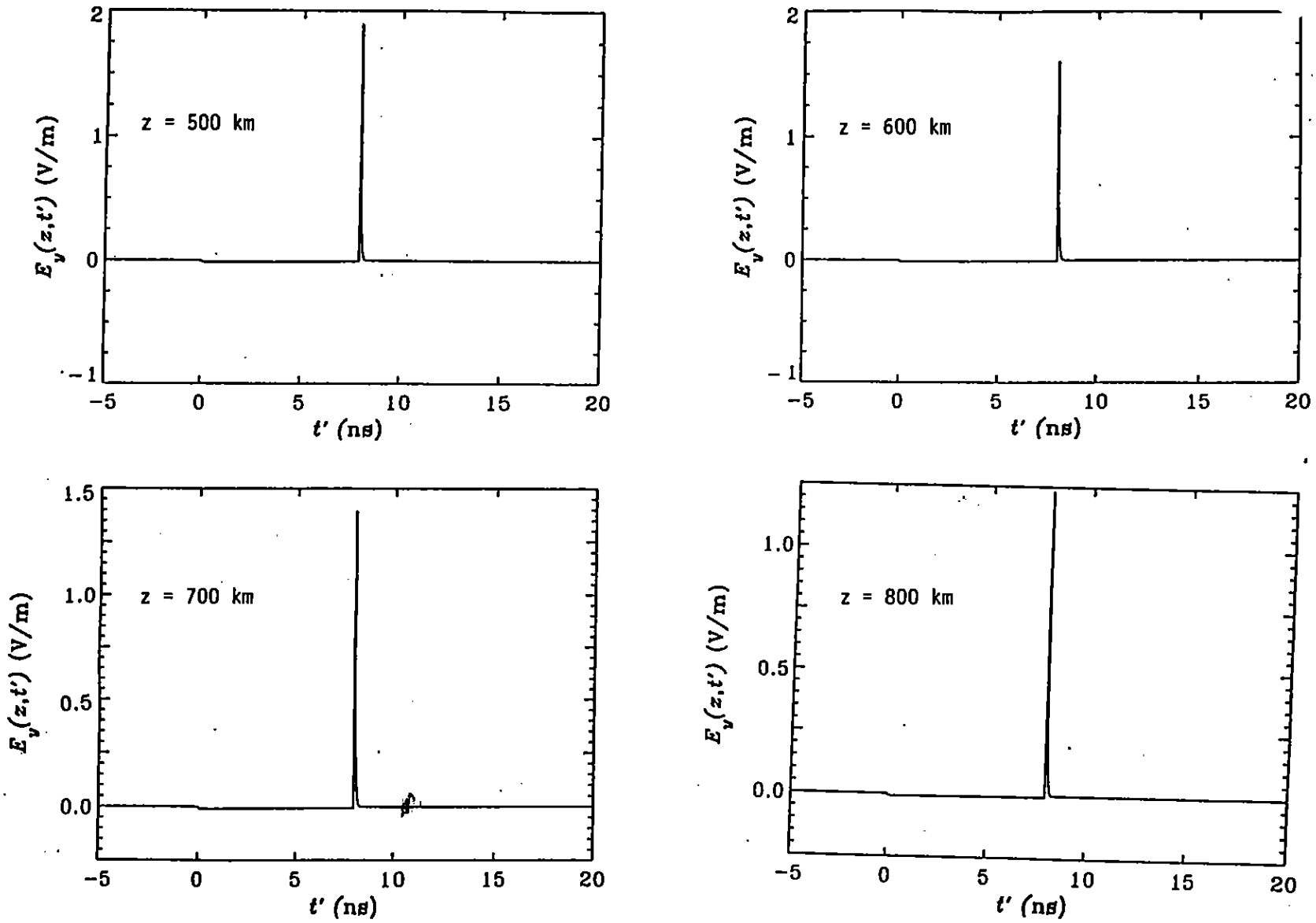

Figure 12. Trans-ionospheric propagation for the case of $N \simeq 1.12 \times 10^6$ elec/m^3 or $\omega_p \simeq 6 \times 10^4$ or $f_p \simeq 9.54$ kHz and $\theta = 0°$

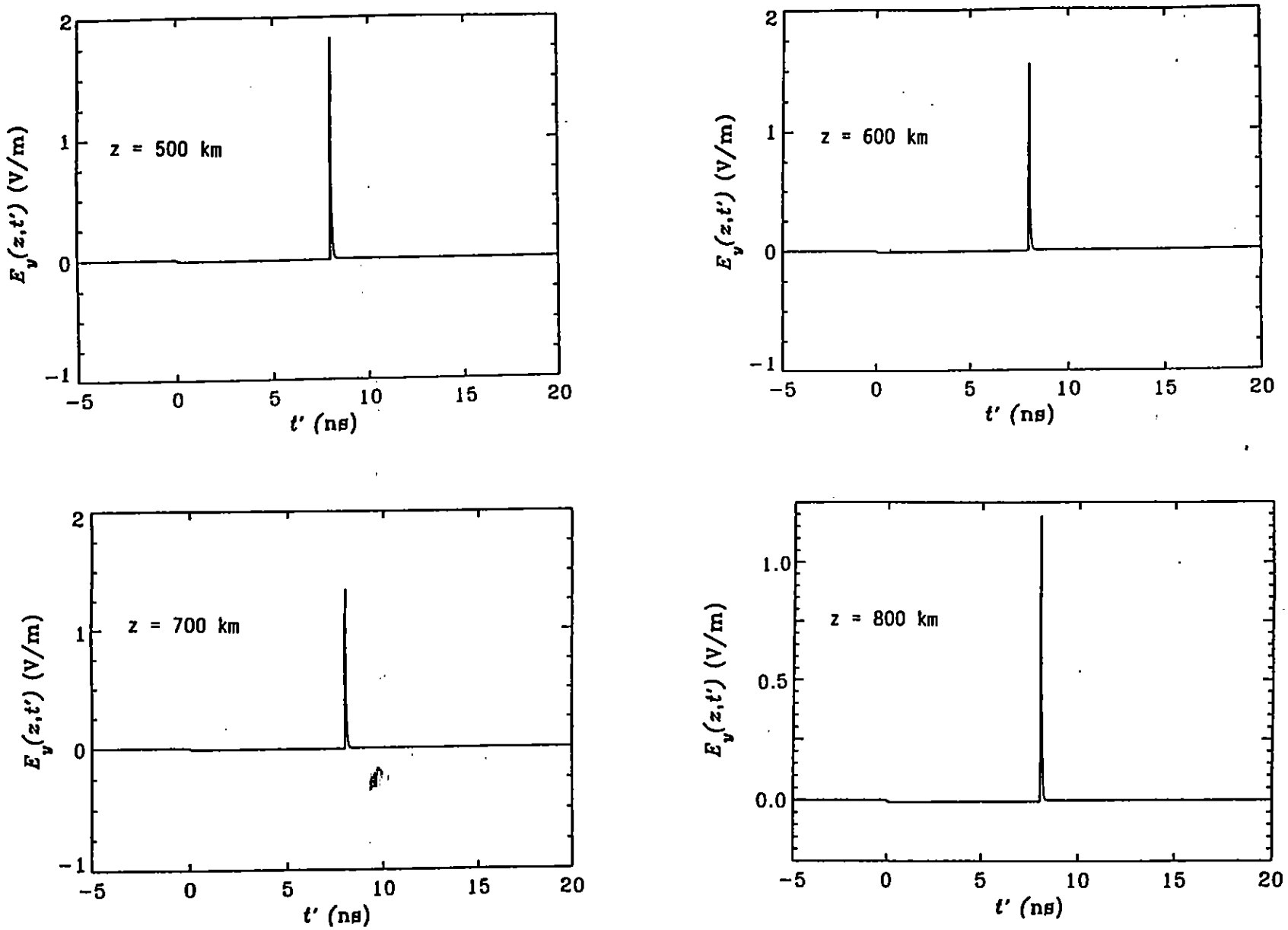

Figure 13. Trans-ionospheric propagation for the case of $N \simeq 1.12 \times 10^6$ elec/m^3 or $\omega_p \simeq 6 \times 10^4$ or $f_p \simeq 9.54$ kHz and $\theta = 15°$

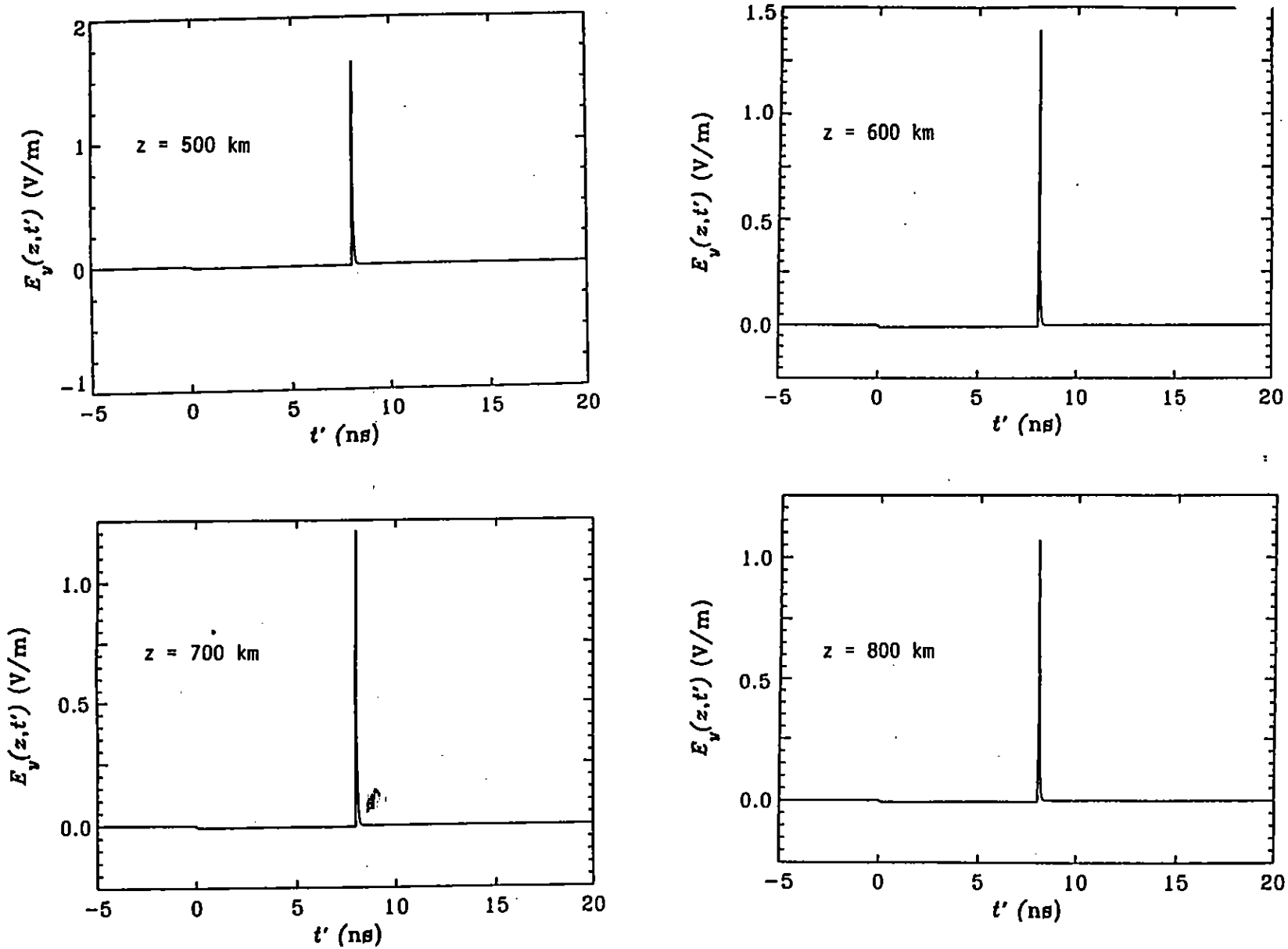

Figure 14. Trans-ionospheric propagation for the case of $N \simeq 1.12 \times 10^6$ elec/m^3 or $\omega_p \simeq 6 \times 10^4$ or $f_p \simeq 9.54$ kHz and $\theta = 30°$

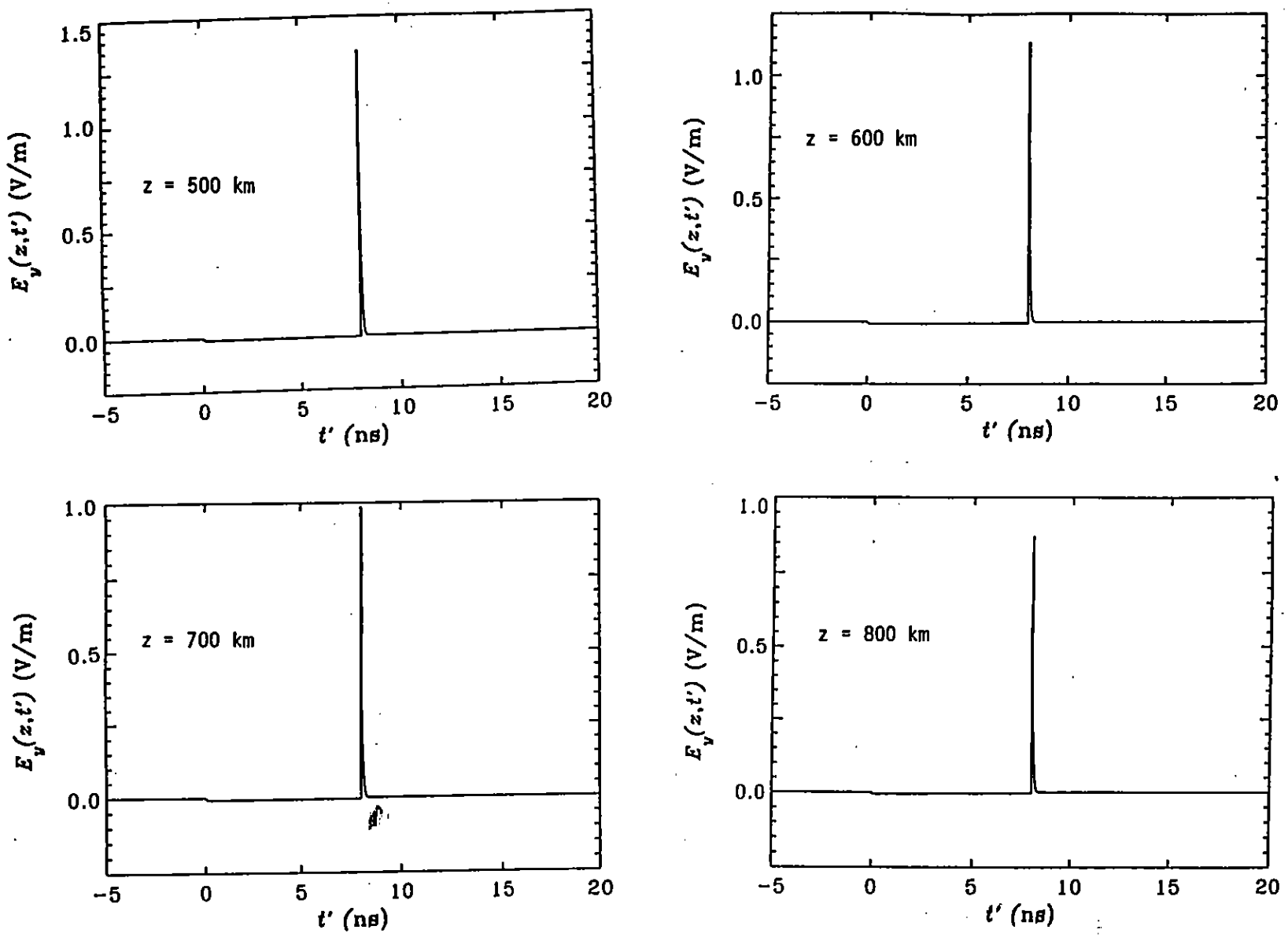

Figure 15. Trans-ionospheric propagation for the case of $N \simeq 1.12 \times 10^6$ elec/m^3 or $\omega_p \simeq 6 \times 10^4$ or $f_p \simeq 9.54$ kHz and $\theta = 45°$

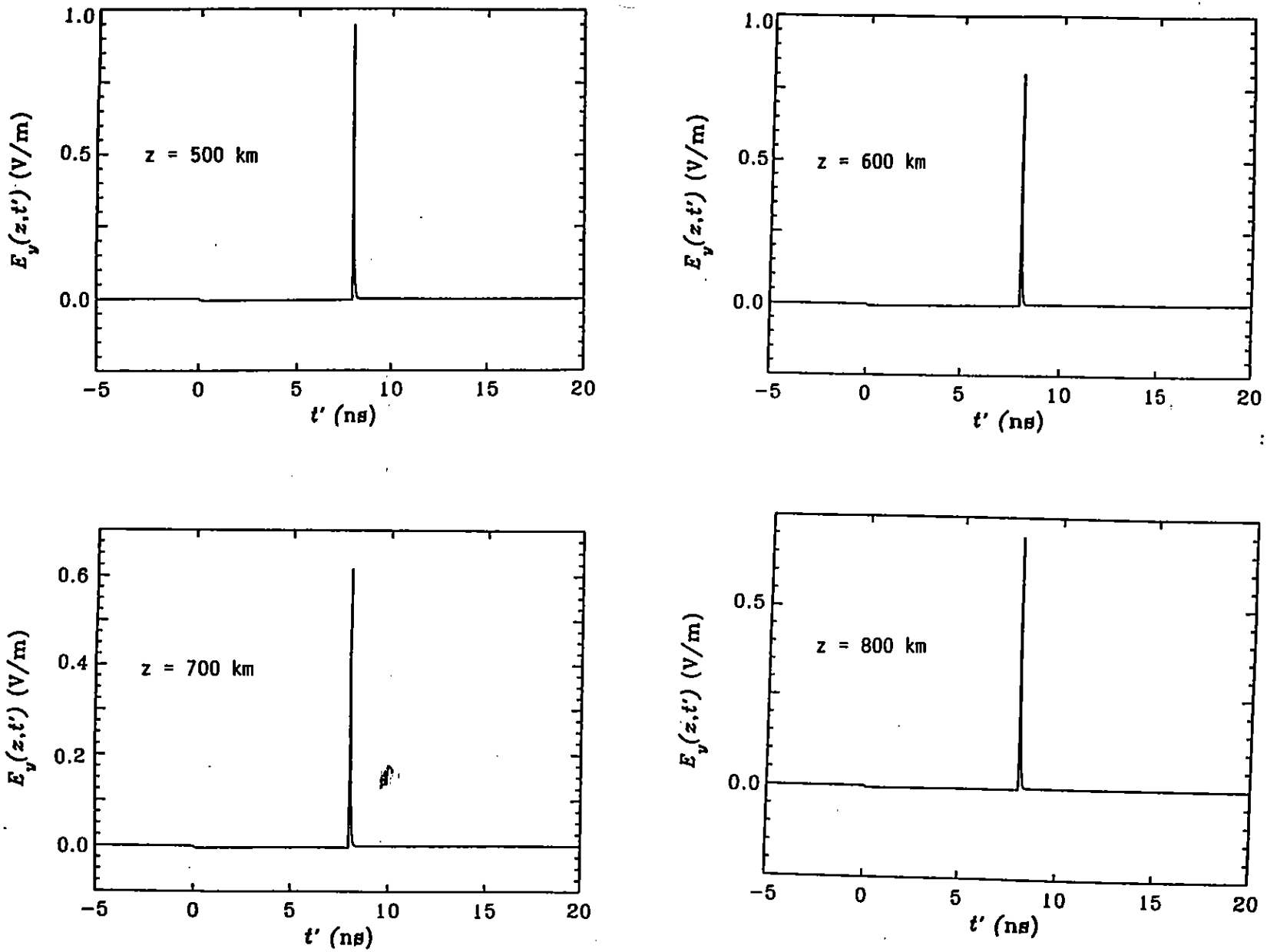

Figure 16. Trans-ionospheric propagation for the case of $N \simeq 1.12 \times 10^6$ elec/m^3 or $\omega_p \simeq 6 \times 10^4$ or $f_p \simeq 9.54$ kHz and $\theta = 60°$

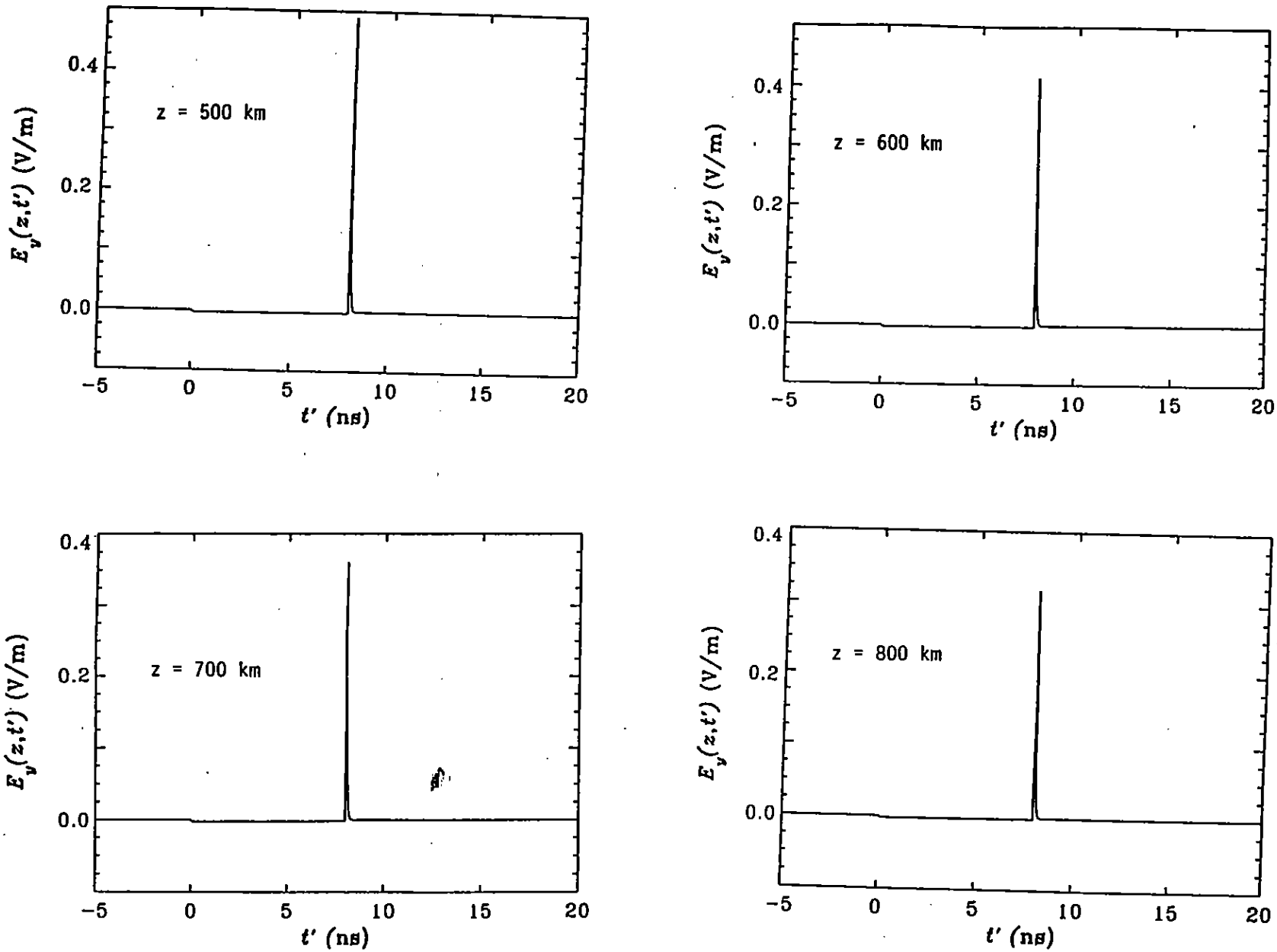

Figure 17. Trans-ionospheric propagation for the case of $N \simeq 1.12 \times 10^6$ elec/m^3 or $\omega_p \simeq 6 \times 10^4$ or $f_p \simeq 9.54$ kHz and $\theta = 75°$

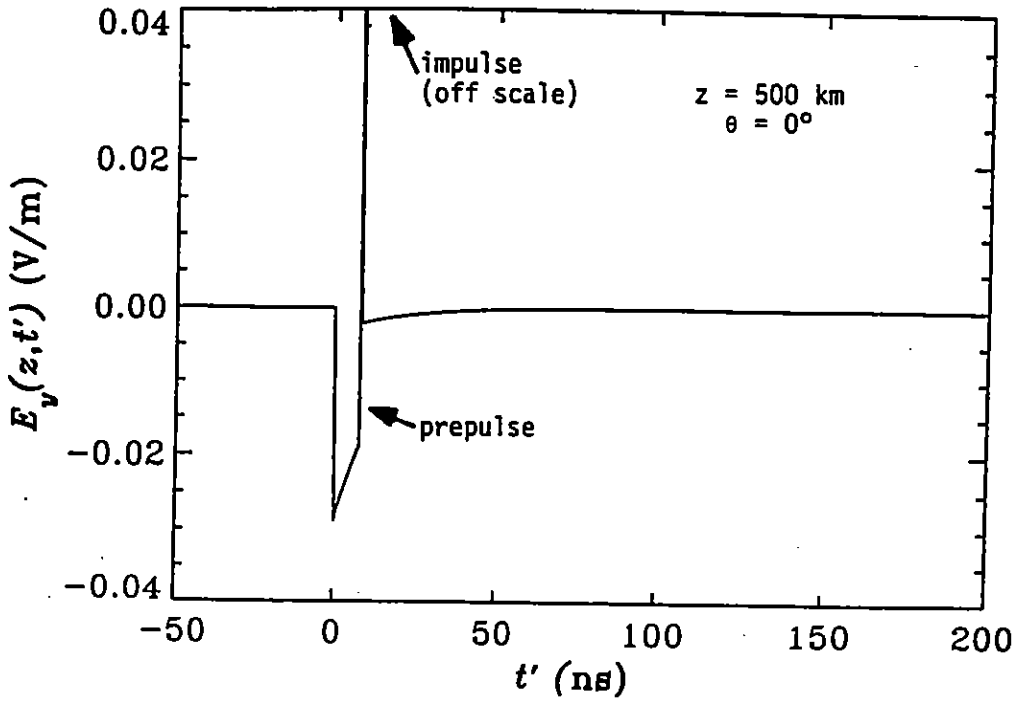

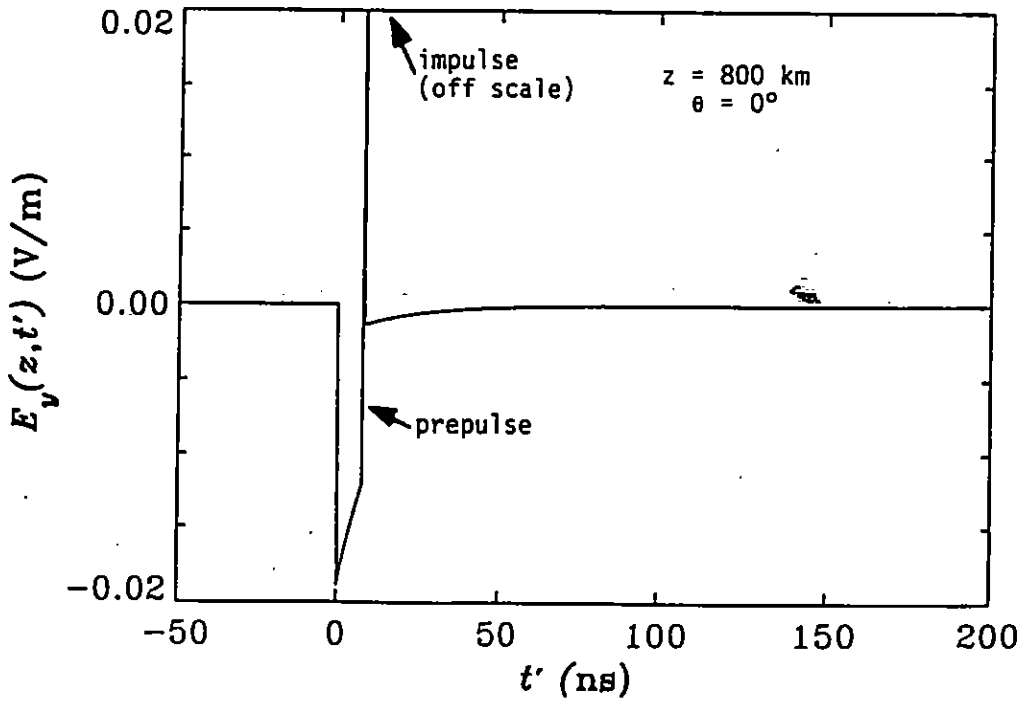

Figure 18. Trans-ionospheric propagation for the case of $N = 1.12 \times 10^6$ elec./m^3 or $\omega_p = 6 \times 10^4$ or $f_p \simeq 9.54$ kHz highlighting the prepulse amplitude and duration

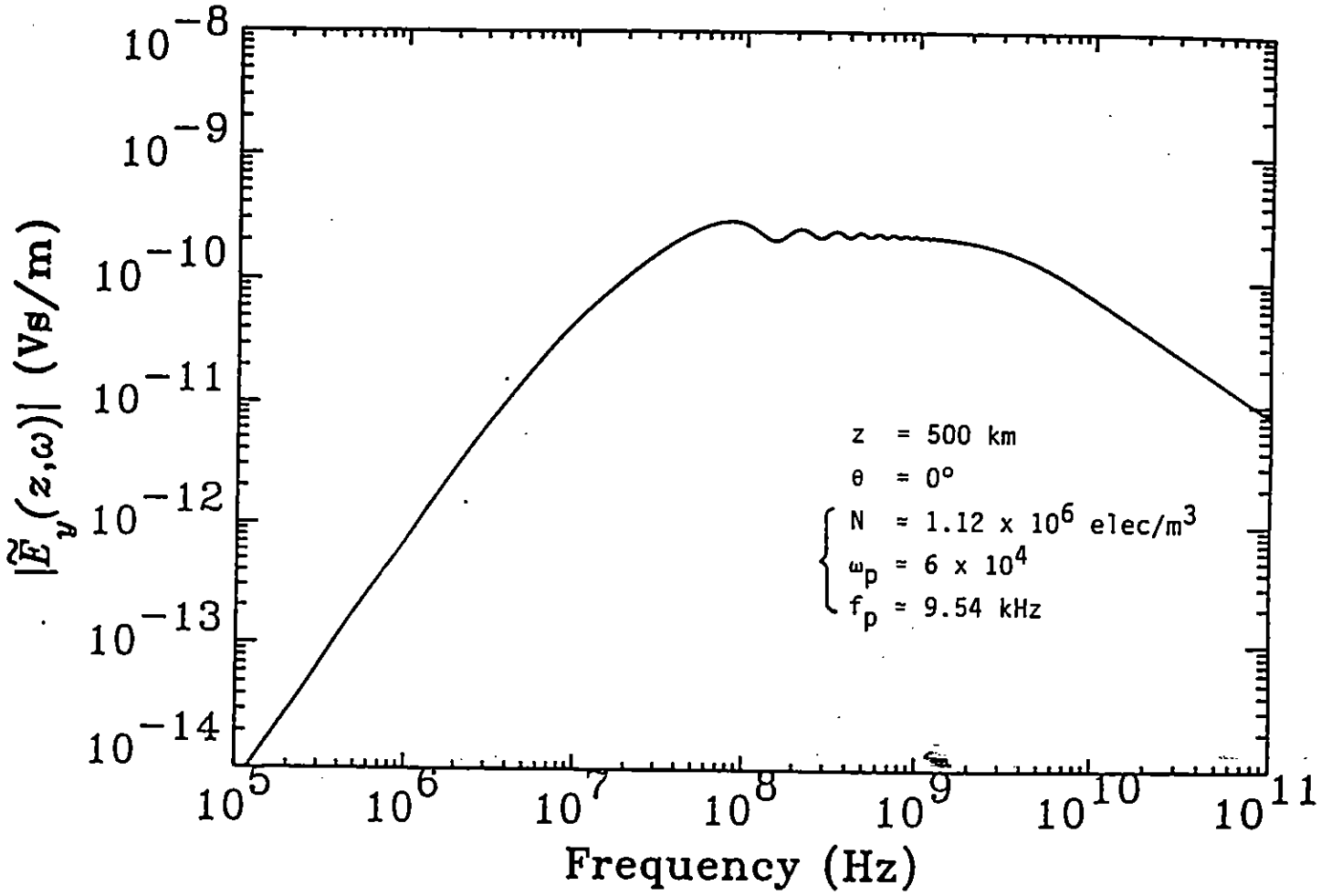

Figure 19. Spectral magnitude of the electric field after trans-ionospheric propagation

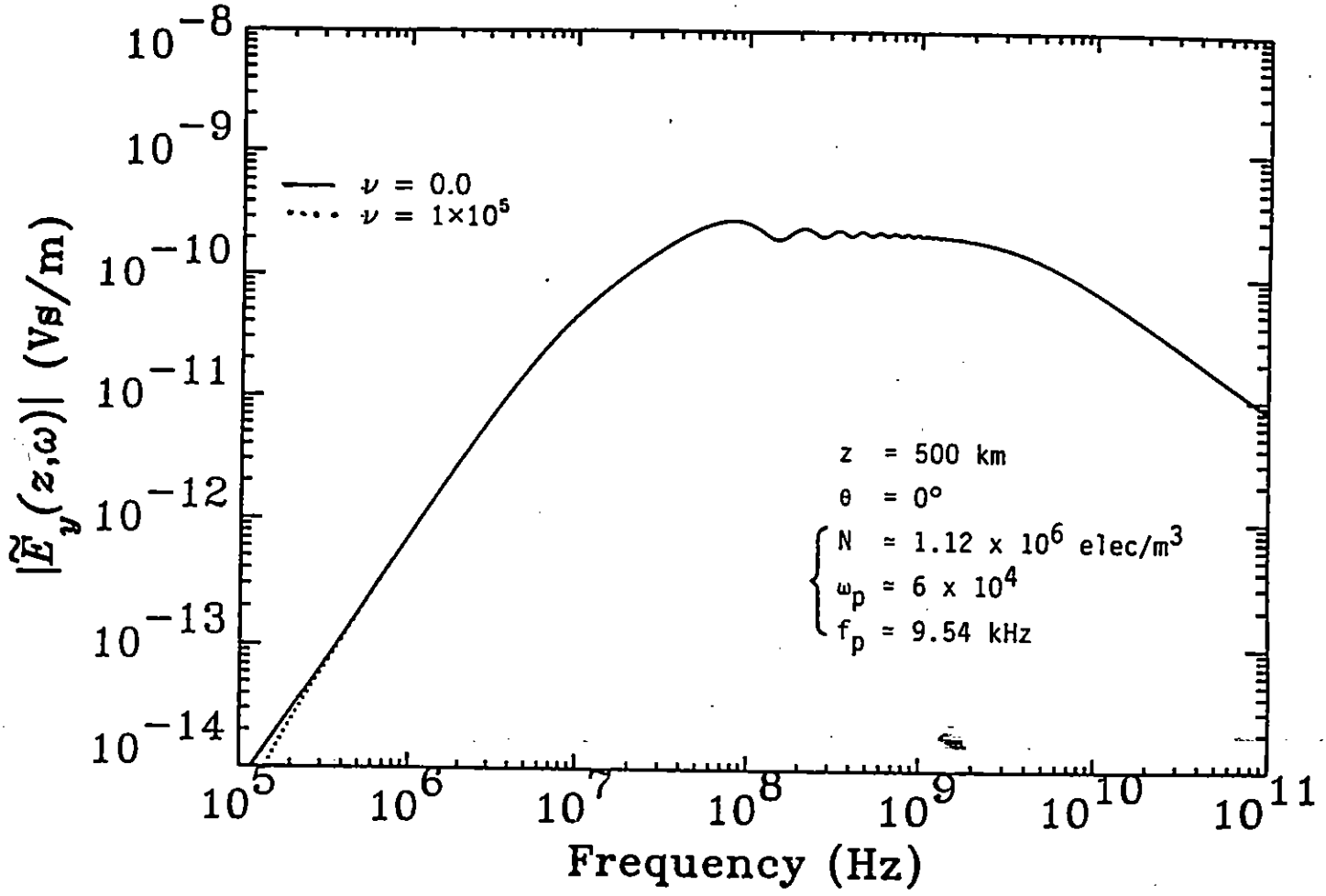

Figure 20. The effect of ohmic losses due to electron collissions on trans-ionospheric propagation ($\nu \equiv$ electron collission frequency Hz)

B. Plasma frequency $f_p \simeq 9.54\ MHz$

This case corresponds to an electron density N of 1.12×10^{12} electrons/m^3 or $\omega_p \simeq 6 \times 10^7$ or $f_p \simeq 9.54$ MHz. As before, we compute both frequency and time-domain signals after trans-ionospheric propagation. The value of N of 1.12×10^{12} electrons/m^3 is the maximum value (see figure 2) for all altitudes and diurnal times. For this value of N, the ionospheric dispersion effects are pronounced. We first display the frequency-domain results in figures 21 to 26 for varying launch angles θ_i. For each launch angle, the distance in the ionosphere is varied from 500 km to 800 km in steps of 100 km. The main feature in these spectral magnitude plots is that the ionosphere acts as a high-pass filter and all of the incident frequencies below the plasma frequency f_p of 9.54 MHz are filtered out or reflected back at the air-ionosphere interface. However, the frequencies above f_p are transmitted and dispersed. The dispersion has a pronounced effect on the time-domain signals shown in figures 27 to 32. Each of these figures is for a particular launch angle θ ranging from 0 to 75° in steps of 15°. The ionospheric path z is varied from 500 to 800 km. For each value of z two time-domain plots are shown. The one on the left goes for a duration of 500 ps, while the one on the left is the initial 20 ps plot. The long-time plot (500 ps) does not resolve the initial positive impulse and hence the 20 ps plot to show the positive going impulse followed by a negative undershoot which is followed by the ringing. The ringing frequency asymptotically approaches the plasma frequency of 9.54 MHz (period $\simeq$ 100 ns). The high-frequencies travel with a larger velocity and arrive at the observer first, according as

$$\text{phase velocity} \quad v_p = \frac{c}{n} = \frac{c}{\sqrt{1 - \left(\frac{\omega_p}{\omega}\right)^2}}$$

$$\text{group velocity} \quad v_g = nc = c\sqrt{1 - \left(\frac{\omega_p}{\omega}\right)^2} \tag{22}$$

For frequencies $\omega \gg \omega_p$,

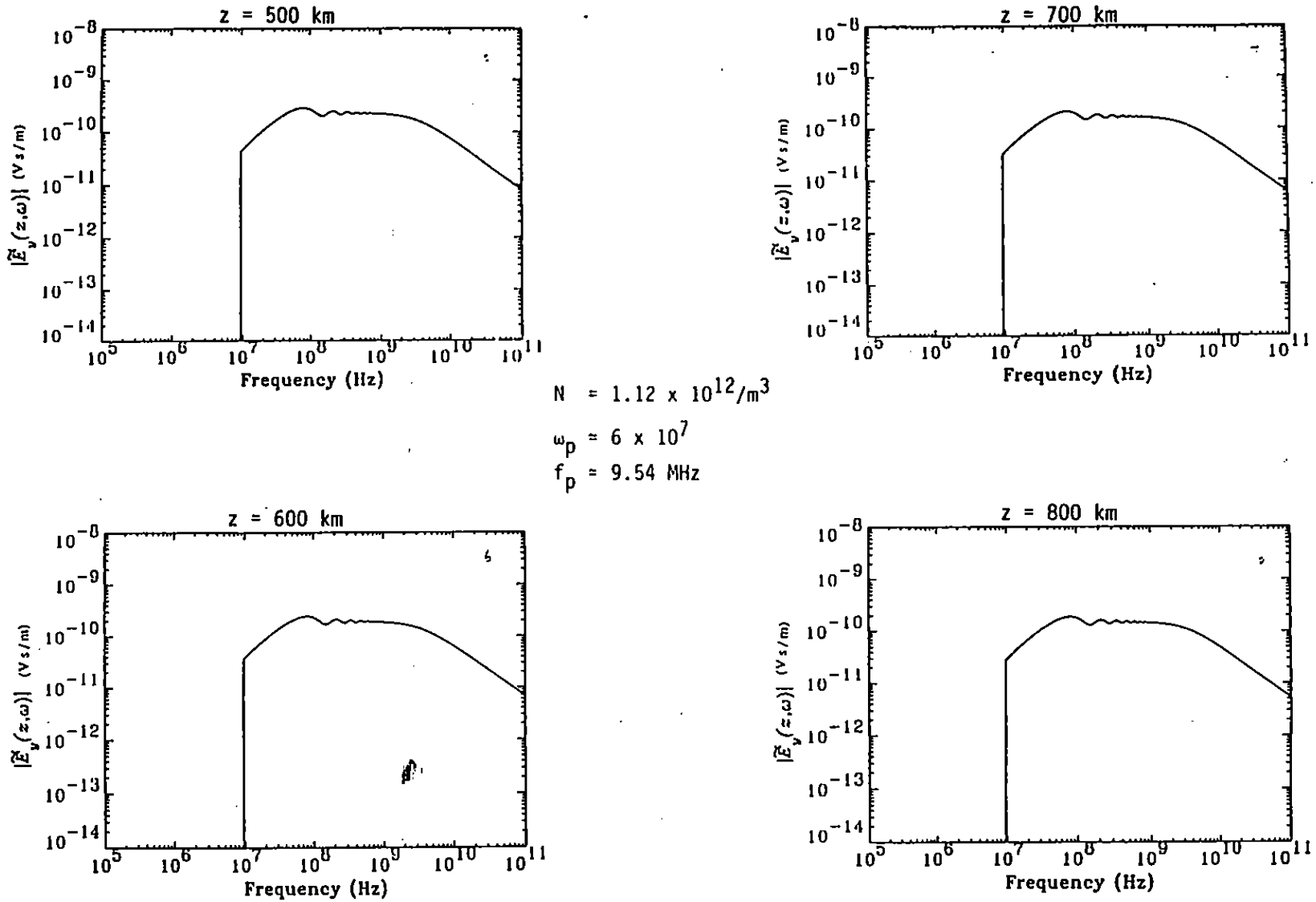

Figure 21. Spectral magnitudes after trans-ionospheric propagation $\theta = 0°$

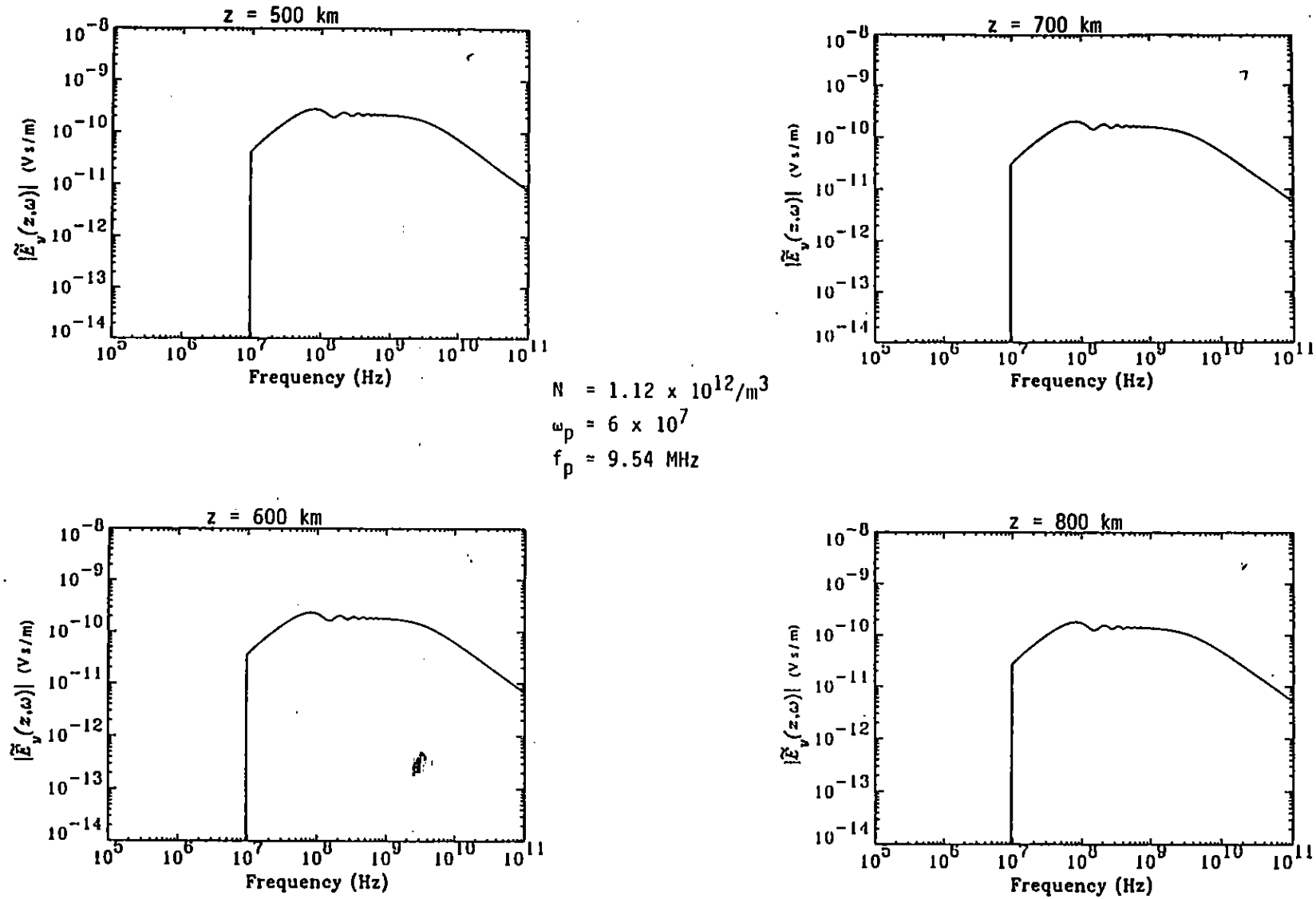

Figure 22. Spectral magnitudes after trans-ionospheric propagation $\theta = 15°$

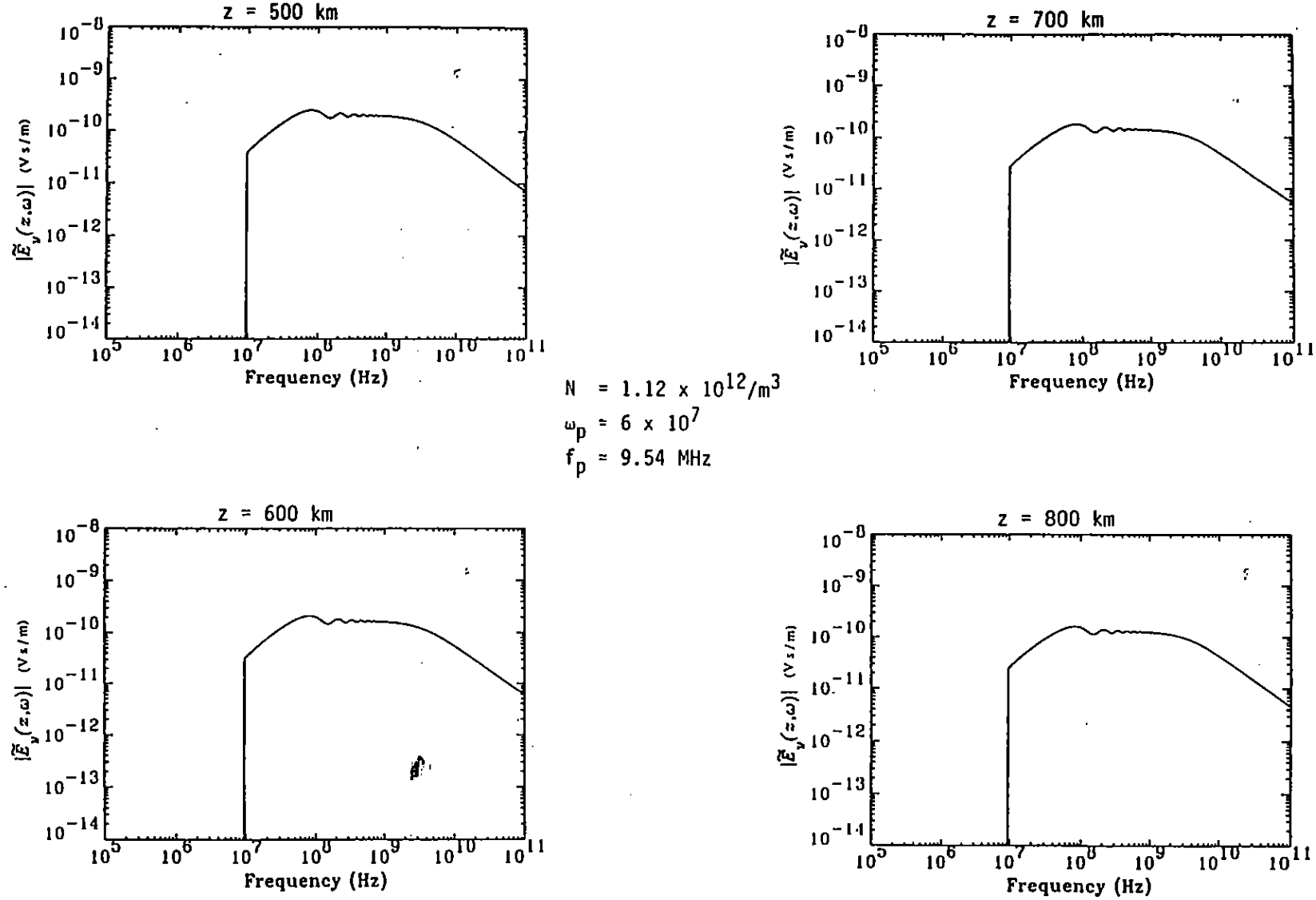

Figure 23. Spectral magnitudes after trans-ionospheric propagation $\theta = 30°$

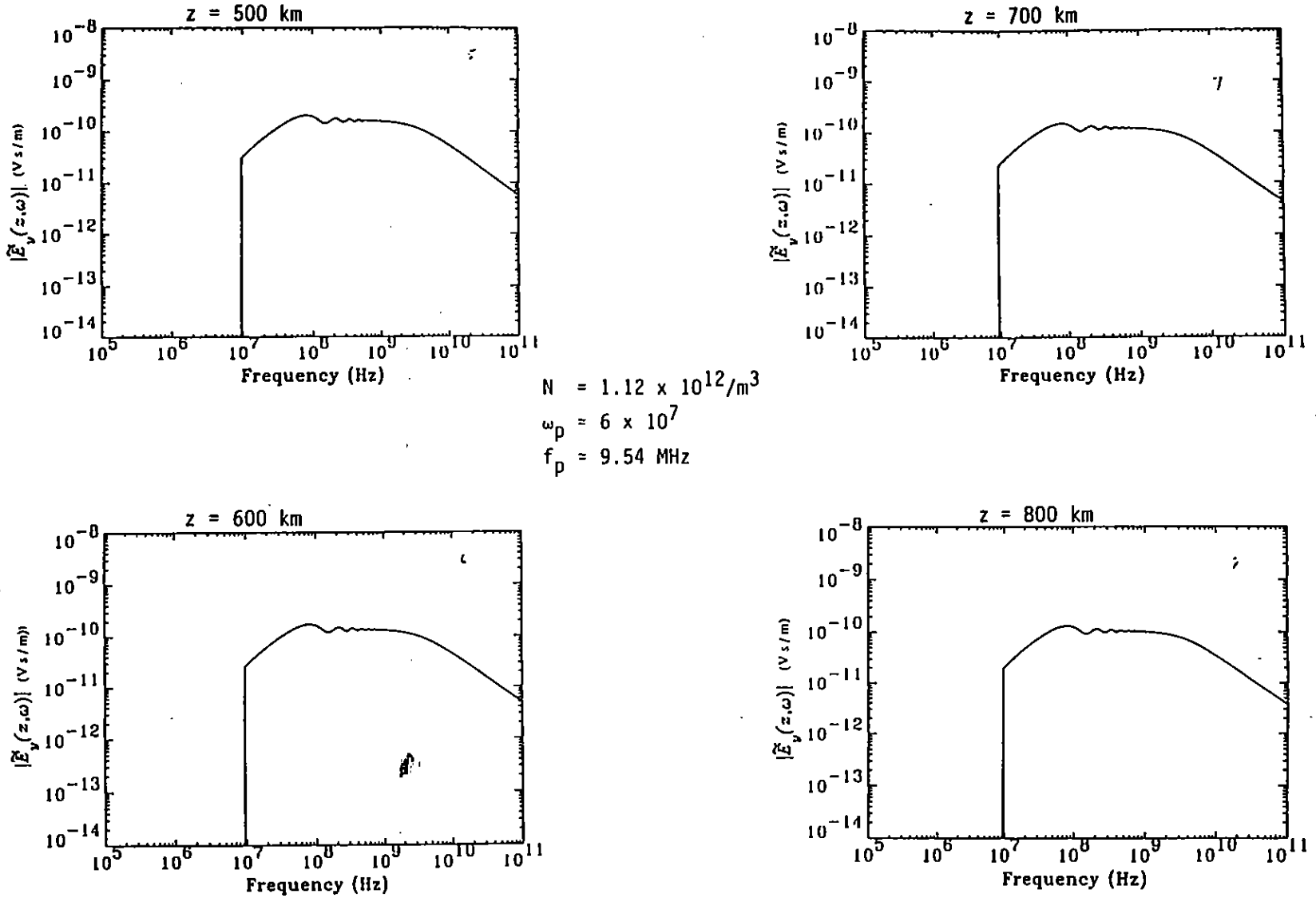

Figure 24. Spectral magnitudes after trans-ionospheric propagation $\theta = 45°$

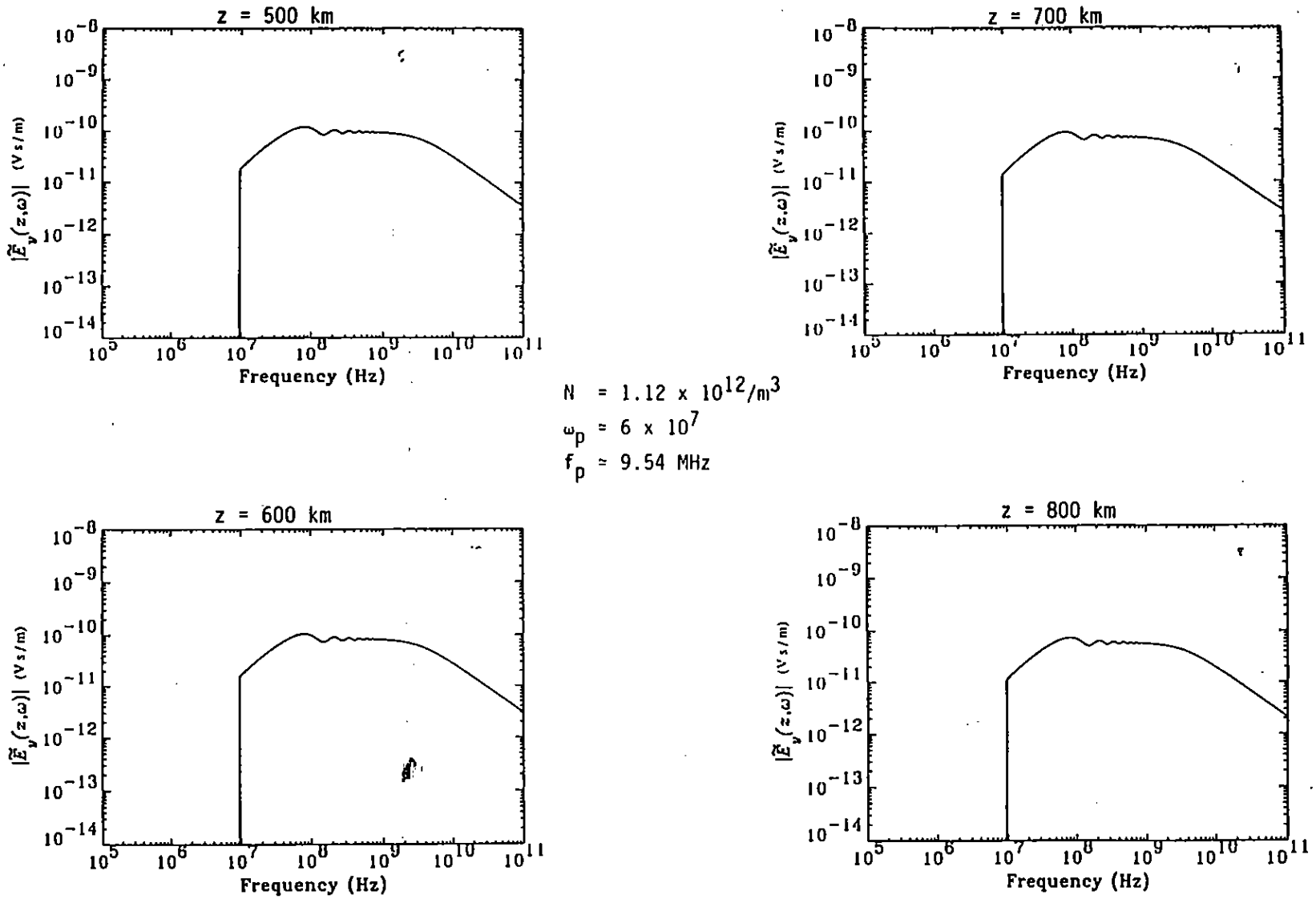

Figure 25. Spectral magnitudes after trans-ionospheric propagation $\theta = 60°$

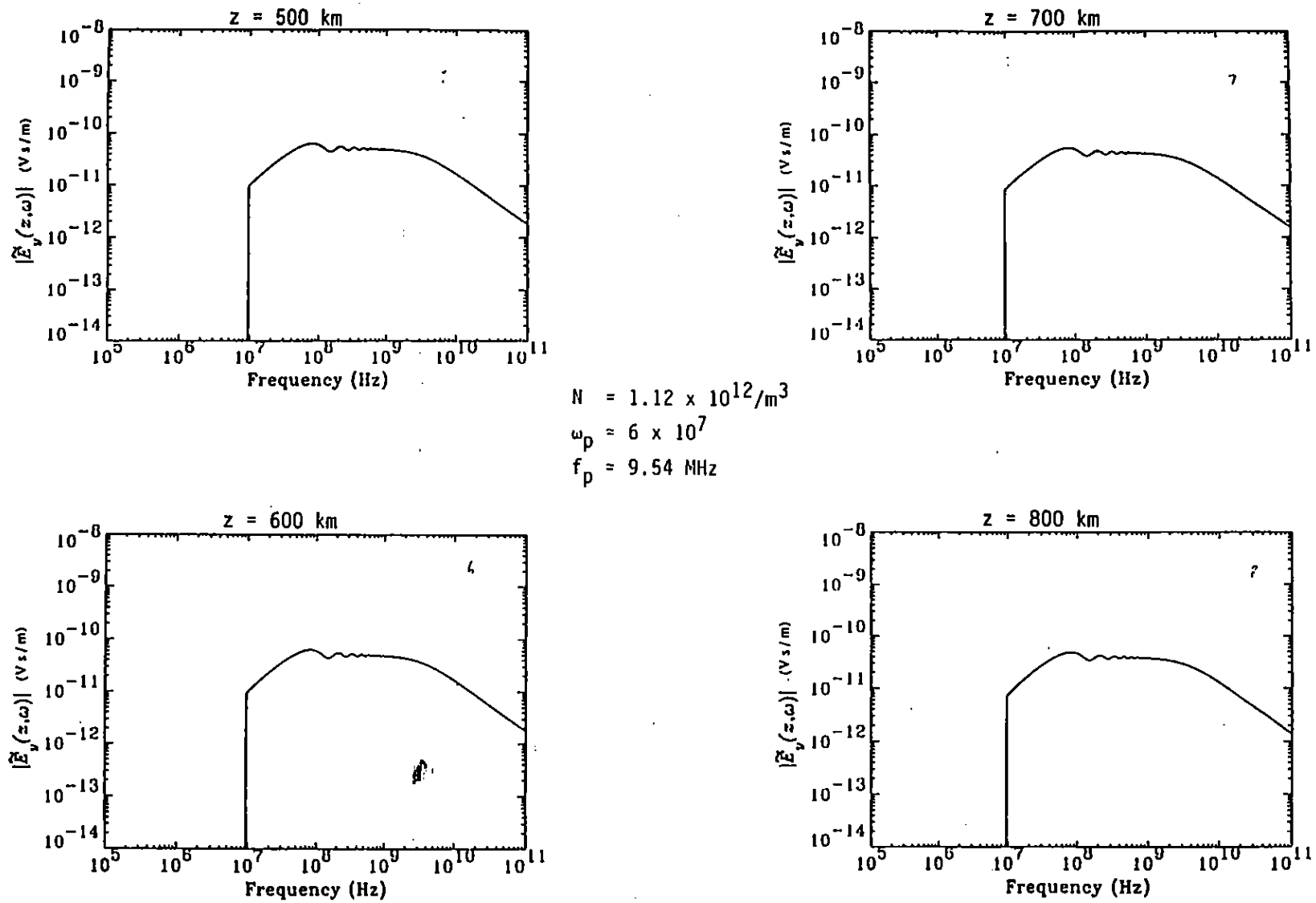

Figure 26. Spectral magnitudes after trans-ionospheric propagation $\theta = 75°$

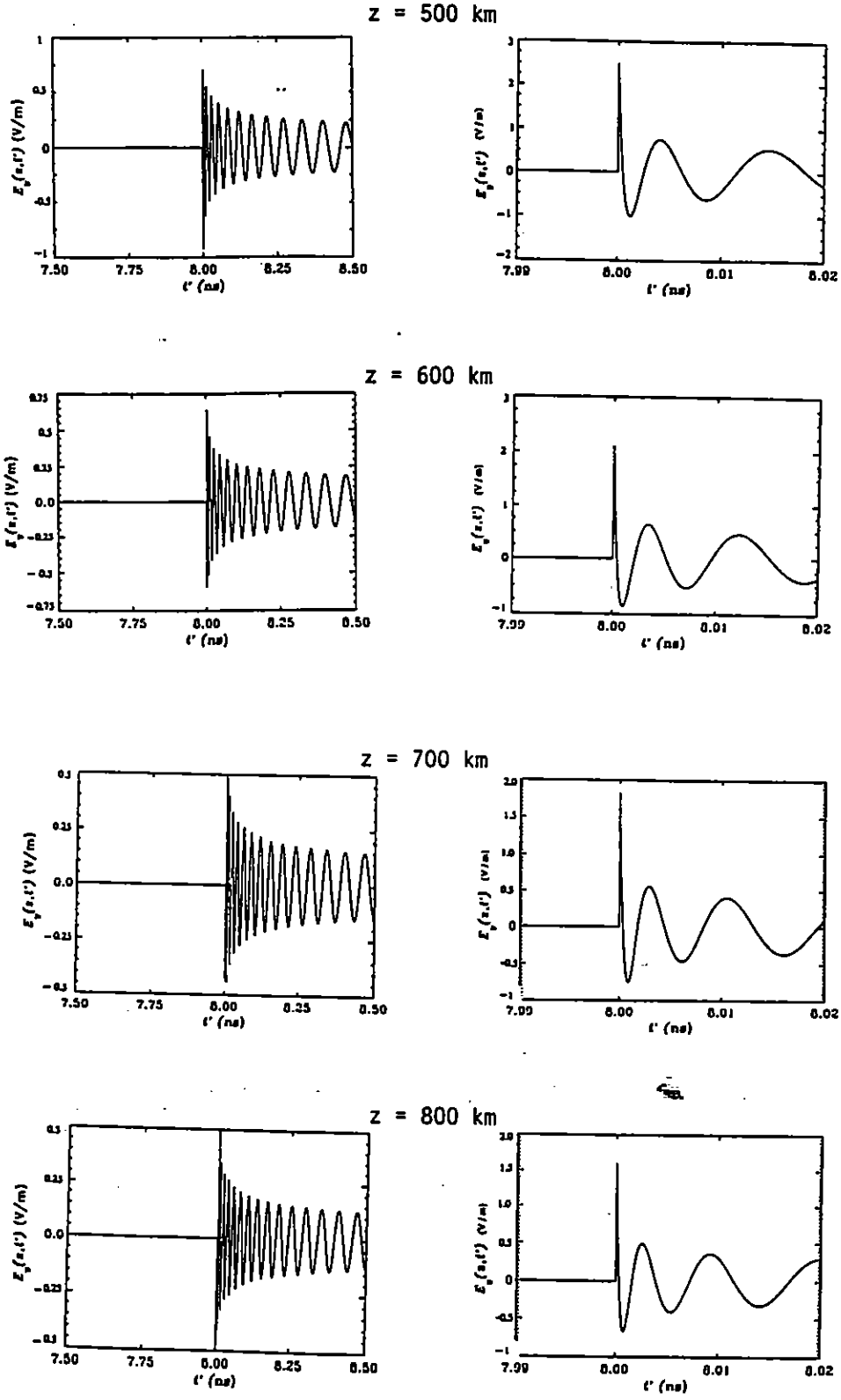

Figure 27. Trans-ionospheric propagation for the case of $N = 1.12 \times 10^{12}$ elec./m^3 or $\omega_p \simeq 6 \times 10^7$ or $f_p \simeq 9.54$ MHz

$$\theta = 0°$$

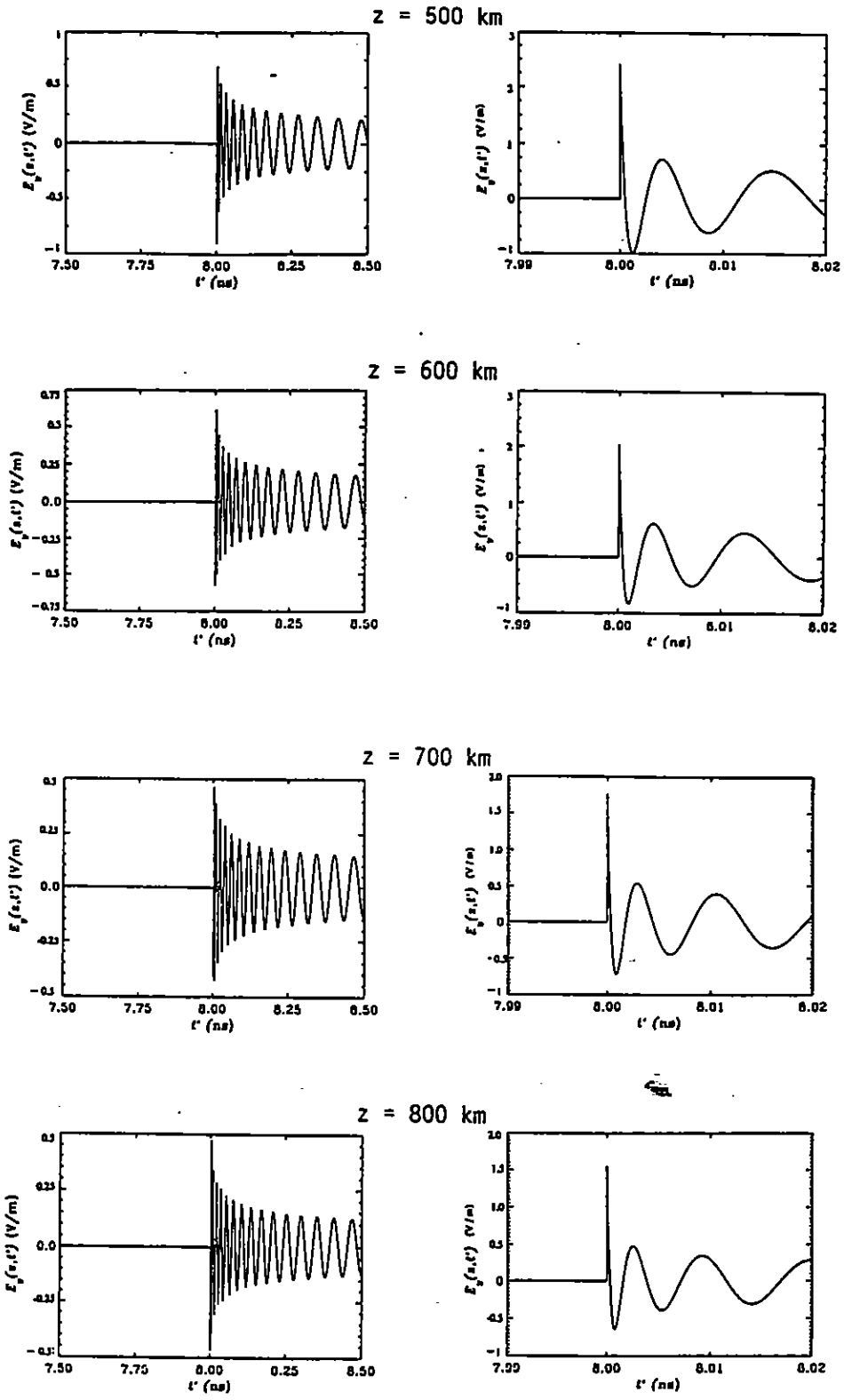

Figure 28. Trans-ionospheric propagation for the case of $N = 1.12 \times 10^{12}$ elec./m^3 or $\omega_p \simeq 6 \times 10^7$ or $f_p \simeq 9.54$ MHz

$$\theta = 15°$$

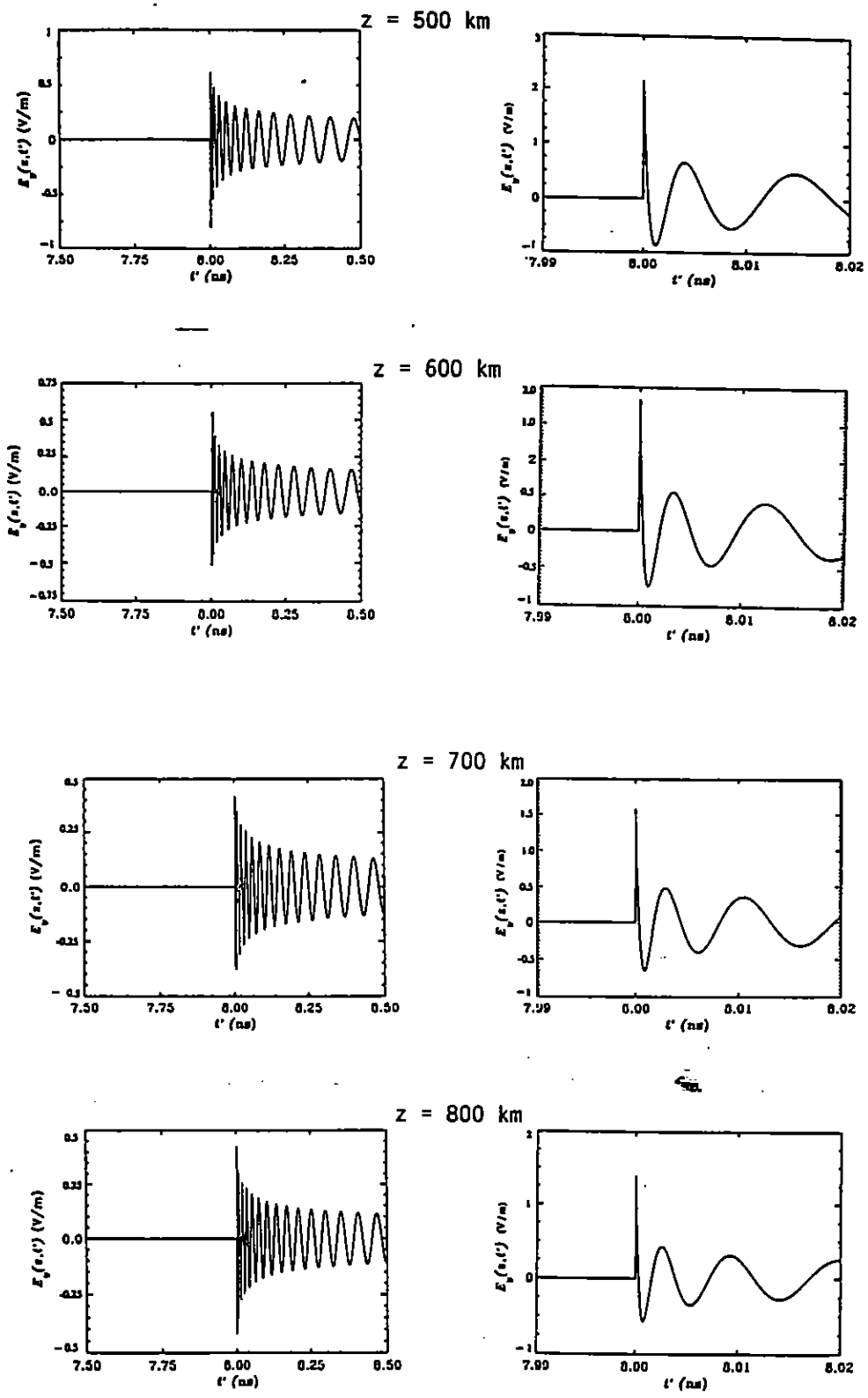

Figure 29. Trans-ionospheric propagation for the case of $N = 1.12 \times 10^{12}$ elec./m^3 or $\omega_p \simeq 6 \times 10^7$ or $f_p \simeq 9.54$ MHz

$$\theta = 30°$$

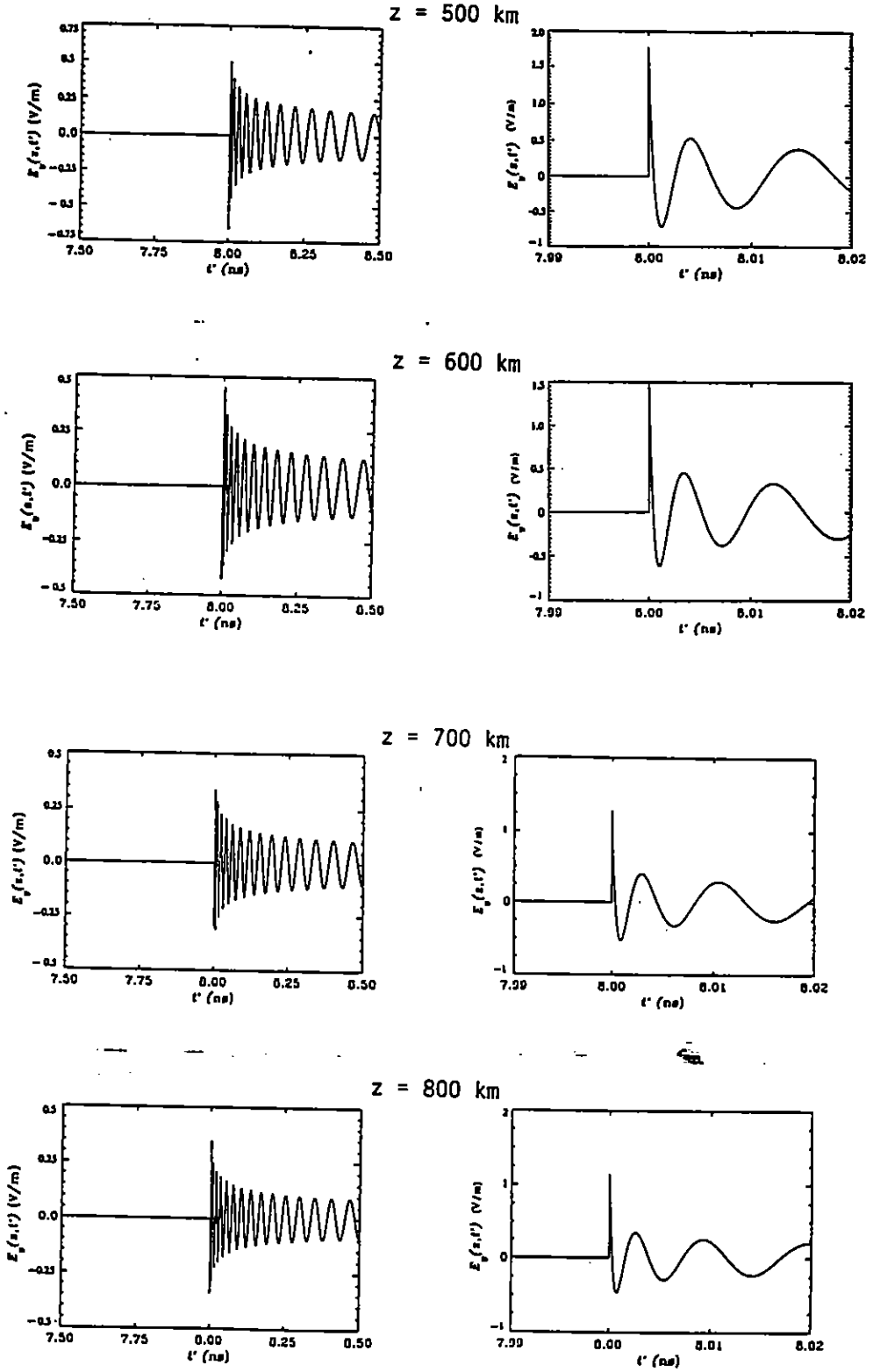

Figure 30. Trans-ionospheric propagation for the case of $N = 1.12 \times 10^{12}$ elec./m^3 or $\omega_p \simeq 6 \times 10^7$ or $f_p \simeq 9.54$ MHz

$$\theta = 45°$$

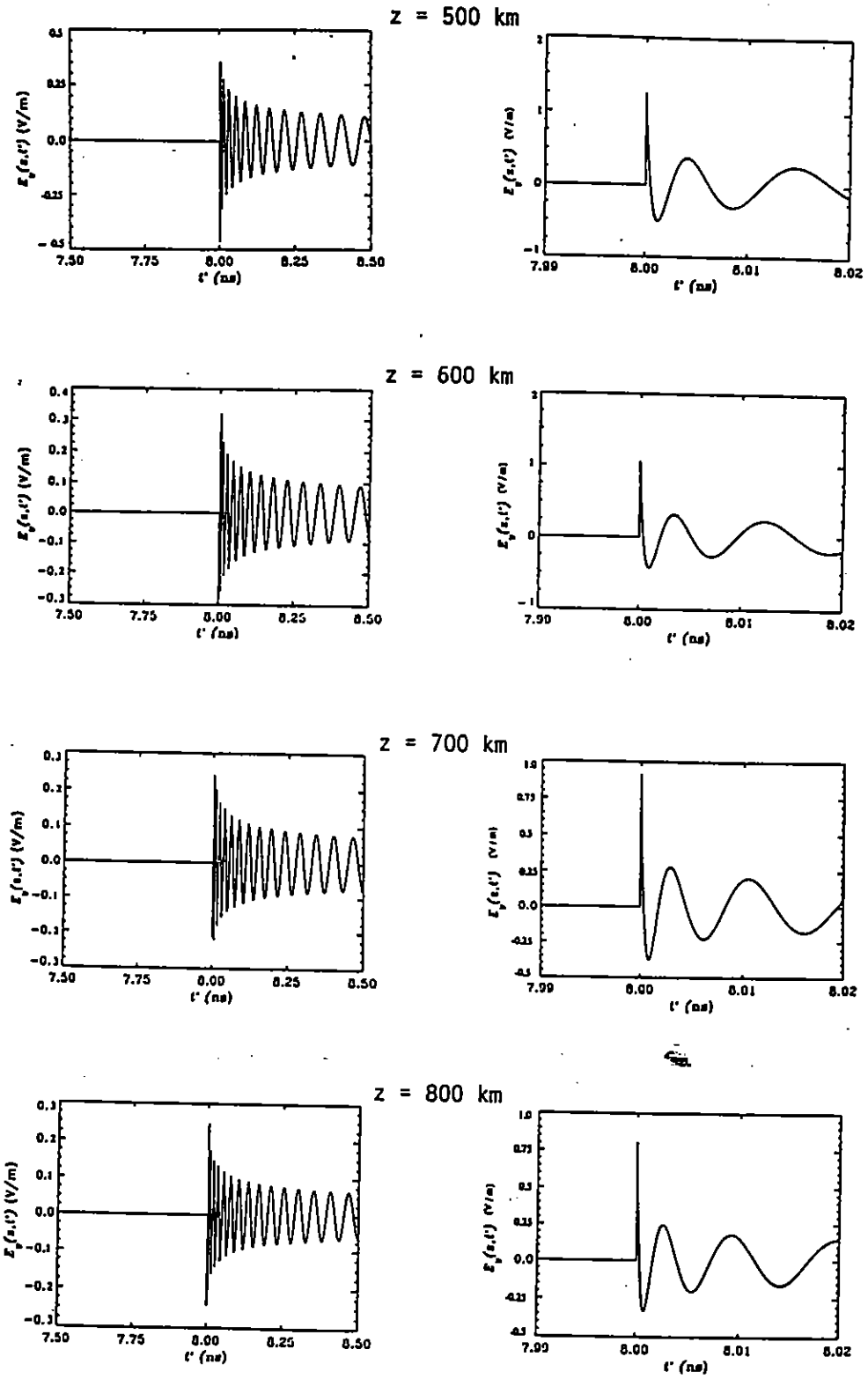

Figure 31. Trans-ionospheric propagation for the case of $N = 1.12 \times 10^{12}$ elec./m^3 or $\omega_p \simeq 6 \times 10^7$ or $f_p \simeq 9.54$ MHz

$$\theta = 60°$$

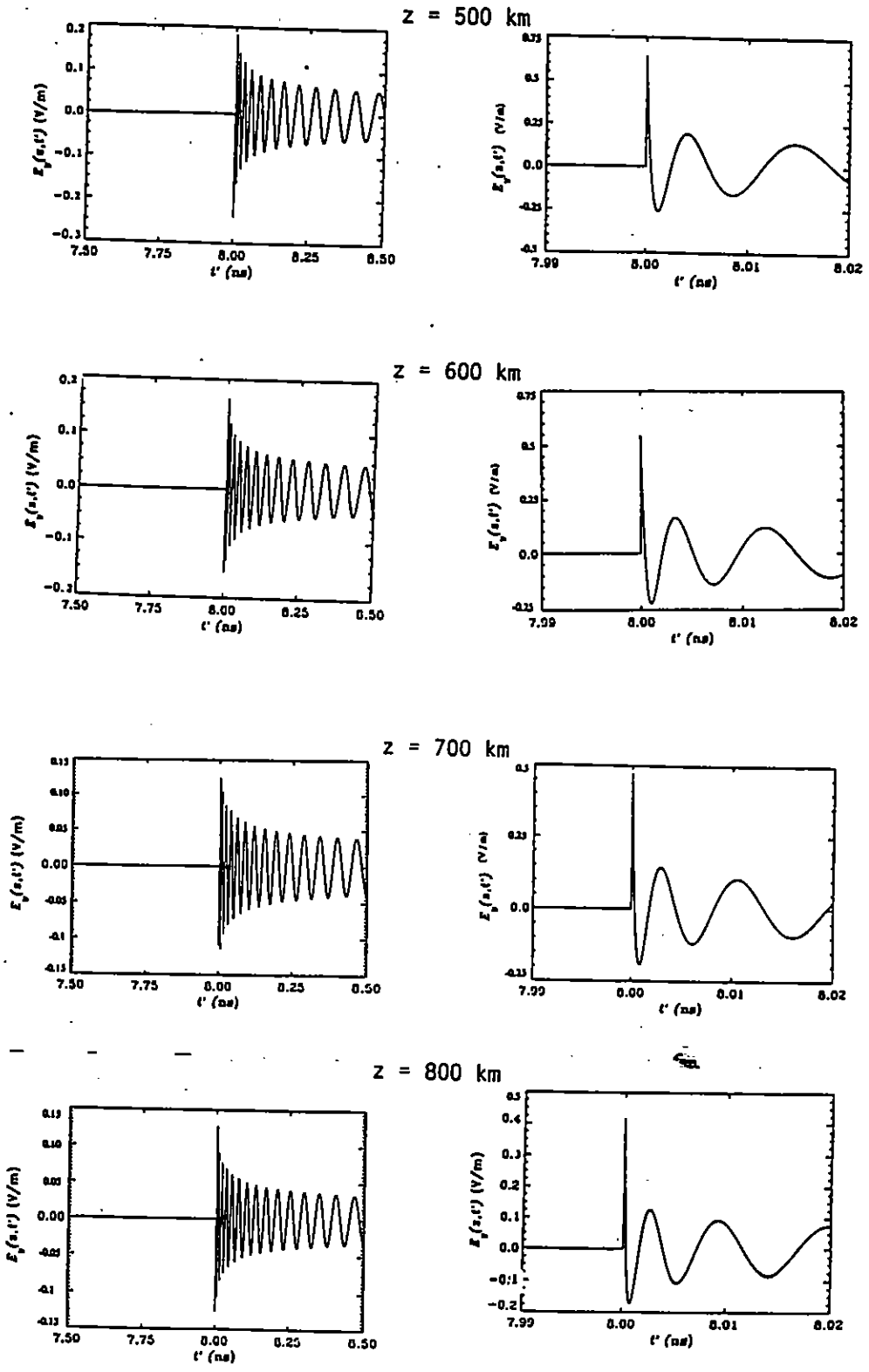

Figure 32. Trans-ionospheric propagation for the case of $N = 1.12 \times 10^{12}$ elec./m^3 or $\omega_p \simeq 6 \times 10^7$ or $f_p \simeq 9.54$ MHz

$$\theta = 70°$$

$$v_p \simeq c\left[1+\frac{1}{2}\left(\frac{\omega_p}{\omega}\right)^2\right]$$
$$v_g \simeq c\left[1-\frac{1}{2}\left(\frac{\omega_p}{\omega}\right)^2\right] \tag{23}$$

The fact that the velocities are frequency dependent leads to the dispersion of a pulse as it propagates through the ionosphere, which is evident in figures 27 to 32.

Next, we turn our attention to the effect of losses shown in figure 33. The losses are easily computed in frequency domain as denoted by (1). As may be seen in figure 33, the losses could be significant up to about 100 MHz, owing to the large propagation distances. However, time-domain fields incorporating the losses are not available. The Fourier inversion of the spectral fields has not yet been possible in closed-form. The numerical Fourier inversion appears to be unstable when such high-frequencies and large propagation distances are involved. Closed-form, time-domain expressions have been possible only under the assumption of no ohmic losses.

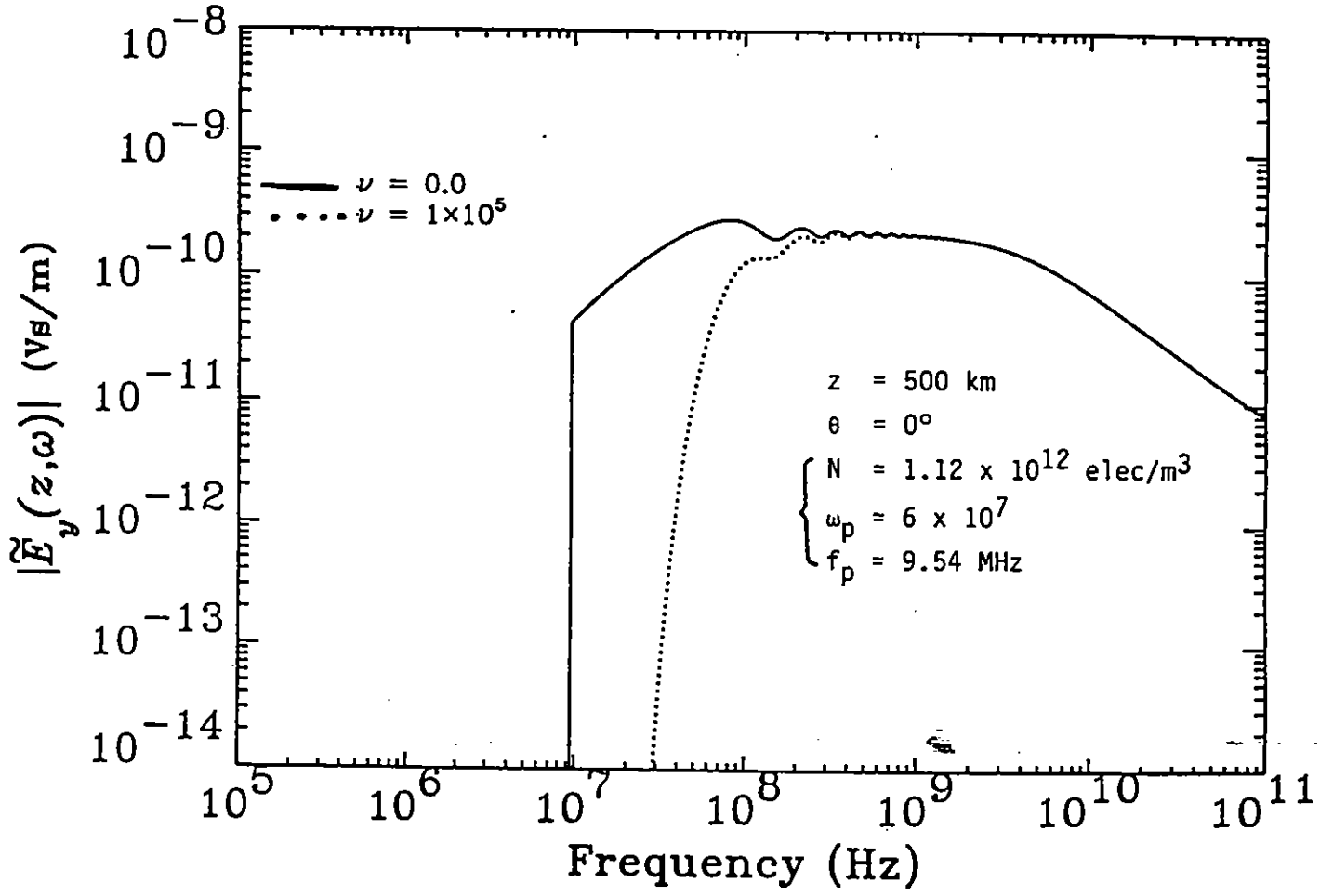

Figure 33. The effect of ohmic losses due to electron collissions on trans-ionospheric propagation ($\nu \equiv$ electron collission frequency Hz)

7. Summary

We have formulated problem of a short-pulse propagation through the ionosphere, modelled by a homogeneous cold-plasma medium. The plasma frequency is fixed at its low and high values. The launch angle from a transmitter on ground and the ionospheric propagation distances are varied. As example transmitter, namely the prototype IRA is considered for an illustrative numerical study. It is found that at the lower value of electron density of $N \simeq 1.12 \times 10^6/m^3$, the short-pulse propagates with almost no dispersion. This corresponds to a plasma frequency of 9.54 kHz. The high-value of $N = 1.12 \times 10^{12}/m^3$ or plasma frequency of 9.54 MHz leads to significant dispersion. The main impulse from the prototype IRA propagates through with a significant compression. In other words, the high-frequencies travel faster to the observer and then the lower frequencies catch up. The effect of ionosphere on the short-pulse is dramatic at this higher electron density.

References

1. M. A. Messier, "A Standard Ionosphere for the Study of Electromagnetic Pulse Propagation," *Theoretical Note 117*, 1 March 1971.
2. S. L. Dvorak and D. G. Dudley, "Propagation of Ultrawideband Electromagnetic Pulses Through Dispersive Media," *IEEE Transactions on Electromagnetic Compatibility*, vol. 37, no. 2, May 1995, pp. 192–200.
3. M. A. Messier, "The Ionospherically Propagated Exoatmospheric EMP Environment," *Theoretical Note 163*, 25 January 1972.
4. R. Roussel-Dupré, "RF Propagation in the Atmosphere; Part 1," Chapter 7 in *Introduction to Ultrawideband Radar Systems*, edited by James D. Taylor, CRC Press, 1995, pp. 325–364.
5. C. E. Baum, "Radiation of Impulse-Like Transient Fields," *Sensor and Simulation Note 321*, 25 November 1989.
6. C. E. Baum and E. G. Farr, "Impulse Radiating Antennas," in *Ultra-Wideband, Short-Pulse Electromagnetics*, edited by H. L. Bertoni, et al., Plenum Press, NY, 1993, pp. 139–147.
7. D. V. Giri, H. Lackner, I. D. Smith, D. W. Morton, C. E. Baum, J. R. Marek, D. Scholfield, and W. D. Prather, "A Reflector Antenna for Radiating Impulse-Like Waveforms," *Sensor and Simulation Note 382*, 4 July 1995.
8. D. V. Giri, "Radiated Spectra of Impulse Radiating Antennas (IRAs)," *Sensor and Simulation Note 386*, 23 November 1995.
9. M. Kelley, *Earth's Ionosphere*, International Geophysics Series, Academic Press, Orlando, 1989.
10. M. Born and E. Wolf, *Principles of Optics*, 6th edition, Pergamon Press, Oxford, U.K., 1980.
11. M. Abramowitz and I. E. Stegun, *Handbook of Mathematical Functions with Formulas, Graphs, and Mathematical Tables*, U.S. Government Printing Office, Washington, DC, 1972.
12. S. L. Dvorak and E. F. Kuester, "Numerical Computation of the Incomplete Lipschitz-Hankel Integral $Je_0(a, z)$," *Journal of Computational Physics*, vol. 87, no. 2, pp. 301–327, 199[illegible]